THE *CASSINI* VISUAL AND INFRARED MAPPING SPECTROMETER (VIMS) INVESTIGATION

R. H. BROWN*, K. H. BAINES, G. BELLUCCI, J.-P. BIBRING, B. J. BURATTI, F. CAPACCIONI, P. CERRONI, R. N. CLARK, A. CORADINI, D. P. CRUIKSHANK, P. DROSSART, V. FORMISANO, R. JAUMANN, Y. LANGEVIN, D. L. MATSON, T. B. MCCORD, V. MENNELLA, E. MILLER, R. M. NELSON, P. D. NICHOLSON, B. SICARDY AND C. SOTIN

Department of Planetary Sciences, 1629 University Boulevard, University of Arizona, Tucson, AZ 85721, U.S.A.

*(*Author for correspondence: E-mail address: rhb@lpl.arizona.edu)*

(Received 5 April 2002; Accepted in final form 2 January 2004)

Abstract. The *Cassini* visual and infrared mapping spectrometer (VIMS) investigation is a multidisciplinary study of the Saturnian system. Visual and near-infrared imaging spectroscopy and high-speed spectrophotometry are the observational techniques. The scope of the investigation includes the rings, the surfaces of the icy satellites and Titan, and the atmospheres of Saturn and Titan. In this paper, we will elucidate the major scientific and measurement goals of the investigation, the major characteristics of the *Cassini* VIMS instrument, the instrument calibration, and operation, and the results of the recent *Cassini* flybys of Venus and the Earth–Moon system.

Keywords: Cassini, Saturn, infrared mapping spectrometer

1. Introduction

The visual and infrared mapping spectrometer (VIMS) is a state-of-the-art, imaging spectrometer that spans the 0.3–5.1 μm wavelength range. It obtains observations of targets in the Saturnian system. These data are used by the team members to carry out many, different, multidisciplinary investigations. These studies, for example, seek to increase our knowledge about atmospheric processes, the nature of the rings, and the mineralogical composition of surfaces.

The VIMS strategy is to measure scattered and emitted light from surfaces and atmospheres. While the spectral domain is emphasized, spatial resolution is also important particularly when it allows the correlation of the spectral characteristics with surface or atmospheric features. Since the spatial domain is important for understanding and interpreting the data, close collaboration is maintained with other, primarily imaging, investigations that are aboard *Cassini*. The addition of data of relatively high-spatial resolution, but of modest spectral resolution, to a data set of high spectral resolution and modest spatial resolution results in synergistic scientific advances well beyond those which could be accomplished using either data set separately. Conversely, very-high spectral-resolution instruments (e.g. CIRS) on

Space Science Reviews **115:** 111–168, 2004.

the *Cassini* spacecraft offer a different set of synergistic interactions for VIMS. Thus, the *Cassini* VIMS investigation will perform much of its work with an eye toward the synergy it has with other experiments.

1.1. Technical Heritage of the VIMS Instrument

The *Cassini* VIMS instrument has its roots in a long line of proposed imaging spectrometers, starting with a rudimentary instrument proposed for the *Lunar Polar Orbiter* in 1974. A more refined concept was proposed for the *Mariner Jupiter Uranus* (MJU) mission in 1975. This design was accepted for the *Jupiter Orbiter Probe* (JOP, later named *Galileo*) Mission in 1977. After selection, this design rapidly evolved into that of the NIMS instrument. Further consideration of these concepts for terrestrial applications led the Jet Propulsion Laboratory to propose to design and develop the airborne visible/infrared spectrometer (AVIRIS) in 1983. In 1987 this system measured its first spectral images (Green *et al*., 1998). Also, in the early 1980's, an instrument development program for future planetary missions was setup at JPL and headed by Larry Soderblom as principal investigator.

This collaboration resulted in several similar instruments optimized for different planetary targets, most notably the OMEGA instrument, the Mars Observer VIMS, and the CRAF VIMS. Mars Observer VIMS and CRAF VIMS are *Cassini* VIMS' most immediate forbearers, but changes made in the VIMS instrument design in response to NASA's demands to reduce the cost of the strawman *Cassini* VIMS resulted in a substantial heritage from Galileo NIMS. Despite that heritage, which goes so far as to include parts from the Galileo NIMS engineering model, *Cassini* VIMS is a substantial step beyond NIMS in the evolution of visual and infrared imaging spectrometers.

This program developed imaging spectrometer designs for the *Comet Rendezvous Asteroid Flyby* (CRAF), the *Mars Observer* (MO), and the *Cassini* missions. While these spectrometers were selected as facility instruments on all three missions, the CRAF mission was cancelled and the MO instrument was removed from the payload in favor of the remaining payload elements that never reached Mars. Only the *Cassini* instrument survived and flew in space.

Cassini VIMS has inherited much from the NIMS instrument, including mechanical and optical parts from the original NIMS engineering model. VIMS nevertheless represents a substantial improvement over the state of the art as marked by the NIMS instrument. In particular, where the NIMS instrument incorporates a moving grating that scans a multiple-order spectrum across a linear array of discrete detectors, the VIMS instrument includes a fixed, multiply blazed grating and array detectors in both its visual and near-infrared channels. Another important improvement is the way the visual and infrared channels scan spatial targets. The VIMS-VIS (visual channel) uses a two-dimensional array detector and a scanned slit (literally scanning a two-dimensional scene across the spectrometer slit) to provide two-dimensional spatial coverage. The infrared channel has only a linear array

of detectors and therefore must use a two-dimensional scanning secondary mirror to obtain the same spatial coverage. The NIMS instrument by contrast scans a scene in only one direction while using the relative motion between the target and the spacecraft to scan the other spatial dimension.

The major differences between the *Cassini* VIMS and the Galileo NIMS lie in the incorporation of a separate visual channel using a frame-transfer, silicon CCD detector with separate foreoptics and analog/control electronics, the inclusion of a radically improved infrared detector with improved order sorting and thermal background rejection, an improved infrared focal plane cooler design, an improved main electronics design, a two-dimensional, voice-coil-actuator-driven, scanning secondary mirror in the infrared foreoptics, a fixed, triply blazed grating in the infrared, a redundant 16-megabit buffer, and a redundant, lossless, hardware data compressor using a unique compression algorithm developed by Yves Langevin. These improvements result in an instrument with substantially greater capability for planetary imaging spectroscopy—so much so that *Cassini* VIMS is the most capable and complex imaging spectrometer presently flying on a NASA planetary spacecraft.

1.2. International Cooperation

The VIMS investigation is truly an international enterprise. The instrument resulted from the best thinking and skill of scientists and engineers in the United States, Italy, France, and Germany. The bonds of cooperation and friendship formed during the design, construction, and testing of this pioneering instrument have now resulted in the closely knit team that is using this instrument to obtain new knowledge about the Saturnian system.

1.2.1. *The VIMS Engineering Team*

The *Cassini* VIMS Development Project began with the *Cassini* instrument selections in November 1990 and ended 30 days after the *Cassini* launch on October 15, 1997. Overall management responsibility was awarded to the NASA Jet Propulsion Laboratory, but soon after that selection, agencies of Italy and France were invited to join the instrument engineering team. In the resulting division of responsibilities, VIMS-VIS (visual spectral region component) was designed and built by *Officine Galileo* in Florence Italy for the *Agenzia Spaziale Italiana* (ASI); the VIMS data compressors and data buffers were supplied by the *Institut d'Astrophysique Spatiale* (IAS) in Orsay, France for the *Centre National de la Recherche Scientifique* (CNRS); and VIMS-IR (infrared spectral region component) was designed and built by the *NASA Jet Propulsion Laboratory* (JPL) in Pasadena, California. JPL also conducted the integration, test, and calibration of the instrument with involvement by the science team and members of all the engineering teams.

Note that throughout this document we denote the visible spectral region component (channel) of VIMS as VIMS-VIS, and the infrared component (channel) as VIMS-IR.

The original VIMS project manager at JPL was Robert F. Lockhart. Mr. Lockhart was later asked to lead the effort to build the entire suite of four *Cassini* facility instruments, including VIMS, and Dr. Gail Klein, then the deputy project manager for VIMS, assumed the VIMS project manager role. David Juergens continued in the role of instrument manager and Edward Miller continued as the senior VIMS system engineer. In Italy, Enrico Flamini of the Agenzia Spaziale Italiana directed the VIMS-VIS Visual Channel (VIMS-VIS) project, with Romeo DeVidi as the VIMS-VIS project manager at Officine Galileo. Francis Reininger served as the Visual Channel system engineer. In France, Alain Soufflot and Yves Langevin led the development of the VIMS data compressor and buffer hardware at IAS.

In total, over 50 engineers in France, Italy, and the US collaborated to design and build the VIMS instrument. The instrument has to date operated flawlessly en route to Saturn, a testament to the cohesion and dedication of the engineering team.

1.2.2. *The VIMS Investigation (Science) Team*

The VIMS Science Team came into existence on November 5, 1990 when the US National Aeronautics and Space Administration announced the selections of the various instrument and investigation teams for the *Cassini* Orbiter. The original VIMS science team consisted of: Robert H. Brown (Team Leader), Kevin H. Baines, Jean-Pierre Bibring, Andrea Carusi, Roger N. Clark, Michael Combes, Angioletta Coradini, Dale P. Cruikshank, Pierre Drossart, Vittorio Formisano, Ralf Jaumann, Yves Langevin, Dennis L. Matson, Robert M. Nelson, Bruno Sicardy, and Christophe Sotin.[1]

There have been some changes since the original selection. Added to team membership were: Alberto Adriani, Giancarlo Bellucci, Bonnie J. Buratti, Ezio

[1]Institutional affiliations are as follows (in alphabetical order by last name): Alberto Adriani (CNR Istituto di Astrofisica Spaziale, Italy), Kevin H. Baines (NASA Jet Propulsion Laboratory), Jean-Pierre Bibring (Universite de Paris Sud-Orsay, France), Giancarlo Bellucci (CNR Istituto Fisica Spazio Interplanetario, Italy), Bonnie J. Buratti (NASA Jet Propulsion Laboratory), Robert H. Brown (University of Arizona, Team Leader), Ezio Bussoletti (Instituto Universario Navale, Italy), Fabrizio Capaccioni (CNR Istituto di Astrofisica Spaziale, Italy), Andrea Carusi (CNR Istituto di Astrofisica Spaziale, Italy), Priscilla Cerroni (CNR Istituto di Astrofisica Spaziale, Italy), Roger N. Clark (U.S. Geological Survey, Denver), Michael Combes (Observatoire de Paris-Meudon, France), Angioletta Coradini (CNR Istituto di Astrofisica Spaziale, Italy), Dale P. Cruikshank (NASA Ames Research Center), Pierre Drossart (Observatoire de Paris-Meudon, France), Vittorio Formisano (CNR Istituto Fisica Spazio Interplanetario, Italy), Ralf Jaumann (Institute for Planetary Exploration, DLR, Berlin, Germany), Yves Langevin (Universite de Paris Sud-Orsay, France), Thomas B. McCord (University of Hawaii, Honolulu), Dennis L. Matson, (NASA Jet Propulsion Laboratory), Vito Mennella (Osservatorio Astronomico di Capodimonte, Italy), Phillip D. Nicholson (Cornell University), Robert M. Nelson (NASA Jet Propulsion Laboratory), Bruno Sicardy (Observatoire de Paris-Meudon, France) Christophe Sotin (Universite de Nantes, Nantes France).

Bussoletti, Fabrizio Capaccioni, Priscilla Cerroni, Thomas B. McCord, Vito Mennella, and Phillip D. Nicholson.[1] Resignations were received from Andrea Carusi, Alberto Adriani, and Ezio Bussoletti.

The VIMS science team members' scientific interests range over three major areas: planetary surfaces, atmospheres and rings. The combined scientific goals of the VIMS scientific team are discussed later in this paper.

2. Scientific Goals of the Vims Investigation

At the time of this writing, the *Cassini* spacecraft has flown by Venus twice, the Earth once, and Jupiter once. Later in this paper we describe some of the observations made for the purposes of instrument test-and-calibration during the Venus encounters and the Earth flyby. Scientific results derived from the flybys of Venus and Jupiter are published elsewhere (Baines *et al*., 2000; Brown *et al*., 2003; McCord *et al.*, 2004). Now we discuss the scientific goals addressed during the cruise phase and orbital tour of Saturn.

2.1. Venus

The specific scientific objectives for Venus arose from VIMS unique ability to peer into Venus' turbulent middle atmosphere as well as the cloud-covered upper atmosphere. Unfortunately, the fact that VIMS-IR was not operational at Venus, combined with the restricted attitude of the spacecraft dictated by the need to protect the *Huygens* probe from excessive insolation, made it impossible to obtain a data set at Venus which would allow us to address the list of scientific goals originally envisioned for Venus. Nevertheless, useful data were obtained with VIMS-VIS. In particular, VIMS-VIS saw the surface of Venus for the first time at multiple sub-micrometer wavelengths, proving that sub-micrometer spectroscopy of the Venus surface is possible. In Section 6 we detail the results obtained during the second Venus flyby (see also Baines *et al*., 2000).

2.2. Jupiter

The VIMS scientific objectives for Jupiter were built upon the results obtained by the Galileo investigations (up until the late fall of 2000). VIMS extended this coverage in time and illumination/emission geometries, as well as provided contiguous spectral coverage into the visual and ultraviolet. Overall, the unique circumstances of the several-month-long *Cassini* fly-by enabled full global maps of Jupiter over both, a large and continuous range of wavelengths spanning nearly the entire solar spectrum, and over a large range of phase angles. Specific VIMS scientific objectives at Jupiter were:

1. Determine the vertical aerosol distributions and microphysical(optical aerosol properties of Jupiter's atmosphere as a function of latitude and longitude.

2. Determine the temporal and spatial variations in constituent gases, including condensables (ammonia, water), and disequilibrium gases (phosphine and ortho/para hydrogen).
3. Investigate the temporal and spatial distribution of lightning, and measure the emission spectrum of lightning from the UV to the near infrared.
4. Determine the vertical and horizontal solar flux deposition in Jupiter's atmosphere to constrain the role of solar energy in Jupiter's meteorology.
5. Investigate auroral and polar haze phenomena, particularly the polar aerosol burden and the abundance of $H_3^+ Z$.
6. Study the temporal evolution of the surfaces of the satellites of Jupiter, particularly that of Io, using VIMS data compared to those of the Galileo NIMS instrument.
7. Investigate time variations in the Io torus.
8. Measure the spectrum of Himalia.
9. Measure the spectrum of Jupiter's Ring.

2.3. The Orbital Tour of the Saturnian System

The overall objectives of VIMS for Saturn and Titan are to investigate ongoing chemical and dynamical processes in a diverse range of planetary and satellite atmospheres, and determine constraints on planetary formation processes and evolutionary histories. The multi-dimensional characteristics of VIMS data acquisition—namely, the ability to acquire two-dimensional spectral maps in 352 wavelengths from the ultraviolet to the thermal infrared allows the instrument to obtain three-dimensional views of atmospheric thermal, aerosol, and chemical structures. Furthermore, these will be over a wide variety of illuminations, and over many emission angles. Meaningful parameters and relationships can be rendered into two-dimensional maps. These then become the tools that enable diverse investigations of chemical, dynamical, and geophysical phenomena. Important targets include the surface and atmosphere of Titan, the cloud-rich atmosphere of the planet itself, its rings, and the plethora of icy moons. Observations of both the day and night sides of these objects shall lead to increased insights into various phenomena involving both reflection and emission of radiation. Occultations of the Sun and stars by these objects should provide new insights into the nature of tenuous stratospheric hazes on Saturn and Titan, the structure of faint rings, and atmospheric composition. Thus, the Saturnian system provides VIMS with many opportunities.

2.3.1. *Titan*

VIMS data will constrain gas and aerosol distributions in Titan's atmosphere as well as their variability with time, and the operative chemical and dynamical processes (Baines *et al.*, 1992). In addition, it is now known that VIMS will be able to see the surface of Titan through atmospheric windows in the infrared (e.g. Tomasko *et al.*, 1989; Griffith and Owen, 1992; Stammes, 1992; Baines *et al.*, 1992; Meier

et al., 2000). Therefore, VIMS studies of Titan will include both the surface and atmosphere and will help in the study of the surface-atmosphere interactions. VIMS objectives for Titan include:

1. Determination of Titan's surface properties using VIMS data obtained at the wavelengths of near-infrared atmospheric windows in Titan's atmosphere (e.g. 0.95, 1.1, 1.3, 1.6, 2.0, 2.7 μm).
2. Measurement of the vertical distribution of condensable and chemically active gas species, including methane, ethane, and acetylene, along with their spatial and temporal variability. In particular, studies of distributions at microbar and millibar levels using stellar occultation measurements.
3. Determination of stratospheric temperature profiles from multispectral occultation measurements.
4. Determination of equipotential surfaces near the 1 mbar level, and inference of geostrophic winds.
5. Determination of vertical aerosol distributions and associated microphysical and optical properties, over latitude/longitude and time. Studies of stratospheric aerosol distributions from stellar occultation measurements.
6. Determination of the bolometric Bond albedo for comparison to CIRS-determined temperature measurements.
7. Determination of the three-dimensional distribution of solar flux deposition rates to constrain the role of solar energy in powering dynamics at various levels, and to constrain the surface solar energy flux over latitude, longitude, and time.
8. Determination of wind fields as revealed by movements of spatially varying clouds and hazes.
9. Determine the composition of Titan's surface, and map that composition as a function of longitude and latitude.
10. Studies of the geology of Titan's surface and any correlation between geomorphology and composition.
11. Searches for signs of active volcanism and tectonism on Titan's surface.

2.3.2. *Saturn*

VIMS will take advantage of the unique geometry of the *Cassini* orbital tour (encompassing both near-polar and equatorial Saturnian orbits) and the 4-year time window to obtain detailed four-dimensional views (i.e. over latitude, longitude, altitude, and time) of Saturn's atmospheric phenomena. Specific VIMS scientific objectives for Saturn include:

1. Determination of vertical aerosol distributions, and associated microphysical and optical properties, over latitude, longitude and time. In addition, provide enhanced accuracy in the determination of stratospheric aerosol properties using stellar occultation measurements.

2. Detection and characterization of spectrally identifiable ammonia cloud features. In particular, determine their spatial distribution and vertical and microphysical properties. Such localized clouds have been identified on Jupiter by Galileo NIMS (c.f., Baines *et al*., 2002). Using similar techniques, their presence on Saturn should be readily observed by *Cassini* VIMS. Also, the detection and determination of water clouds (recently identified in infrared observations by Simon-Miller *et al*., 2000) will be attempted.
3. Determination of the vertical distributions of variable gas species, including condensables (ammonia and perhaps water) and disequilibrium species (phosphine and ortho/para hydrogen), over latitude, longitude and time. Follow the lead of Galileo NIMS (e.g. Roos-Serote *et al.*, 1999, 2000) in such analyses. In addition, study hydrocarbon and other gas distributions at microbar and millibar levels using stellar occultation measurements.
4. Determination of stratospheric temperature profiles from multispectral occultation measurements.
5. Determination of equipotential surfaces near the 1 mbar level, and inference of geostrophic winds.
6. Determination, over time, of wind fields near the ammonia cloud tops and, perhaps, lower-lying clouds as probed by near-infrared wavelengths. Constrain vertical wind components from cloud top altitude variations.
7. Improve the determination of the bolometric bond albedo of Saturn, and use in constraining the magnitude of Saturn's internal heat source.
8. Investigation of the three-dimensional distribution of lightning, and measurement of the emission spectrum of lightning from the UV to the near infrared.
9. Place constraints on chemical/dynamical mechanisms from spatial/temporal variability in atmospheric phenomena. Specifically, investigate links between disequilibrium and condensable gas variations, as well as variations in cloud opacities and vertical distributions.
10. Determination of the three-dimensional solar flux deposition rate to constrain the role of solar energy in powering dynamics at various levels.
11. Investigation of links between polar aerosol burden and composition, and magnetospheric phenomena utilizing charged particle flux estimates from *Cassini* plasma investigations.

2.3.3. *Icy Satellites*

Objectives for the icy satellites are:

1. Determine or constrain the mineralogical compositions of the satellite surfaces at maximum spatial resolution.
2. Determine the composition of the Iapetus dark side material and constrain the origin and evolution of Iapetus and its surface.
3. Relate the compositions of Saturn's icy satellites to that of icy satellites of other planets (i.e. Jupiter, Uranus, Neptune, Pluto)

4. Constrain the insolation absorbed by the satellites of Saturn and thereby constrain the photometric and thermal properties of their regoliths.
5. For the smaller Saturnian satellites, obtain spectral data for comparison with the larger satellites, the ring system, and other small bodies of the outer Solar System.
6. Determine the composition of any dark material on Saturn's satellites, especially Iapetus, Hyperion and Phoebe, and relate the composition of this primitive/organic material to that on other solar system bodies, and to groundbased measurements of objects thought to have primitive material on their surfaces as well as to relevant laboratory data.

2.3.4. *Rings*
Ring objectives are:

1. Determine or constrain the mineralogical composition and grain-size distribution of small (micrometer-sized) as well as large (millimeter- and larger-sized) particles in the rings of Saturn using absorption features found in reflected solar radiation. For rings that are optically thin, constrain, map variations in, and determine the size distribution of small (micrometer-sized) particles via multi-wavelength optical-depth measurements obtained from stellar and solar occultations.
2. Map the radial, azimuthal, and vertical distribution of ring material using stellar occultations, at radial resolutions of 0.1–1 km.
3. Probe dynamical phenomena responsible for ring structure and evolution, including density and bending waves, wakes due to embedded satellites, and resonantly forced ring edges and narrow ringlets, using multiple stellar occultation profiles.
4. Characterize the size distribution of ring particles by imaging the diffraction aureole during stellar occultations.
5. Establish the surface properties (grain size, degree of crystallinity, packing, etc.) of the bodies composing the rings using spectral reflectance measurements.
6. Set bounds on the insolation absorbed by the rings, and thereby constrain their photometric and thermal properties.
7. Determine the composition of any dark material in Saturn's rings and relate its composition to that of other primitive/organic material elsewhere in the solar system and in the laboratory.

3. Measurement Goals

3.1. Surfaces

3.1.1. *Spectral Imaging*
The measurements required to meet the scientific objectives for surfaces can be divided into four broad classes:

Type S1: High-spectral- and low-spatial-resolution data acquired at great distances from the target. These data will provide orbital phase spectral information and will permit longitudinal mapping of the object at scales greater than 5° spherical lunes. Such observations, performed shortly after arrival at Saturn will provide a preliminary database for defining the spectral regions to be studied during subsequent targeted encounters.

Type S2: Observations with high spectral and modest spatial resolution on approach to a targeted satellite encounter until the object fills one VIMS field of view, or until mosaicing is required to obtain full areal coverage. The spatial resolution in this case ranges from ∼10 to ∼20 km. This will provide the best global coverage at highest spectral resolution.

Type S3: Observations with the highest spatial and spectral resolution allowing coverage of the entire illuminated hemisphere of the object in a limited time. In essence, this amounts to constructing the highest spatial resolution map at full spectral resolution in the shortest possible time consistent with the constraints of a given flyby. These types of observations will usually be made during targeted icy satellite flybys far enough ahead of closest approach that full coverage of the object can be made. The spectral ranges and resolutions and targeting will be the product of tradeoffs determined during observations of *Types S1* and *S2* above.

Type S4: High spatial and spectral resolution observations with limited coverage. This type of observation will occur near closest approach during a "close" flyby of an object. This observation type concentrates on obtaining high spatial resolution (at the expense of areal coverage). In practice, we envision riding along with the imaging science subsystem (ISS) and producing a complete VIMS image for each narrow-angle camera frame taken by the ISS. In terms of specific observations of objects in the Jupiter and Saturnian systems, the following discussion of essential observations is presented as a minimal requirement to fulfill the goals of this investigation. As the requirements of the total mission develop and are addressed, this list of observations will be augmented, particularly through obvious resource economies such as joint observations with other instruments.

3.1.2. *The Galilean Satellites*

Although the spatial resolution attained by VIMS during the *Cassini* Jupiter flyby was limited to at best 1 pixel at closest approach, VIMS was able to provide information in the visual and near IR spectral range that was not obtained by either Voyager or the Galileo NIMS spectrometer. During the Jupiter flyby, a full set of *Type S1* observations of the Galilean satellites were obtained. The reader is referred to Brown *et al.* (2003) for a discussion of the results.

3.1.3. *The Saturnian Satellites*

The Phoebe flyby, prior to the start of the *Cassini* orbital tour, will permit observations of *Types S1* through *S3*. Observations will commence in *Type S1* and end up in *Type S3* depending upon the closest approach distance.

The *Cassini* orbital tour will provide a variety of opportunities for *Type S1* observations of the icy Saturnian satellites at solar phase angles from near zero to the maximum solar cone angle constraint (∼160–170°). The minimum requirement is that these observations be made on both hemispheres of all objects at 5° increments in solar phase angle and orbital phase angle. The close satellite encounters will permit *Types S2*, *S3* and *S4* observations of each object. This will yield the near complete spectral mapping of each satellite. Significant support imagery from the ISS will be required for the success of this investigation, much of which will occur as a matter of course as a result of these data being taken simultaneously with the imaging data (VIMS-imaging ride-along mode).

Many *Type S1* observations will be made of Saturn's satellites in order to construct full solar and orbital phase curves. This can be done at times of low spacecraft activity, reducing competition for spacecraft resources.

The typical, targeted satellite flyby will be so fast that, in the time required for a complete VIMS frame to be taken, large changes in phase angle will occur. In addition, the size of the target will change by a large factor. The high spatial resolution data obtained will be a singular event for best definition for subsequent compositional mapping done in concert with ISS NA images. During the period of such an encounter, continuous images will be taken beginning with sub-pixel spatial resolution through the time of closest approach.

3.1.4. *Titan*

During each flyby of Titan, VIMS observations can commence several hours before closest approach. Titan's surface can be mapped at the wavelengths of near infrared windows in Titan's atmosphere. *Type S4* observations will be performed in order to obtain increasing spatial resolution as *Cassini* gets closer to Titan. Mosaics composed of four images taken approximately 4 h before closest approach will allow complete coverage of Titan's hemisphere. Different integration times will be used to measure the opacity of Titan's atmosphere at the wavelengths of near-infrared windows in Titan's atmospheric spectrum. A resolution of about 10 km per pixel can be achieved at 0.5 h before closest approach. A high-resolution mosaic of Titan's surface can be obtained using *image cubes* obtained on successive flybys. This information will complement the observations of Titan's surface by other *Cassini* instruments and will allow the creation of a geological map of Titan's surface based on all *Cassini* observations.

Observations obtained during the first Titan flyby will help characterize the landing site of the *Huygens* probe. Also, at wavelengths longward of 3 μm, it will be possible to map temperature variations expected to result from any ice diapirs exposed at Titan's surface. It may also be possible to sense the release of volatiles from the interior of the satellite. Lenticulae on Europa are features attributed to ice diapirs and have diameters around 10 km. Such a resolution can be obtained by VIMS about half an hour before closest approach. Therefore, such observations during selected flybys will be carried out so as to characterize such

areas. In addition to observations dedicated for VIMS, we will acquire observations while other imaging instruments have control of the spacecraft pointing.

3.2. Atmospheres of Saturn and Titan and Atmosphere Modes

For atmospheres there are two major types of measurement objectives with respect to Saturn and Titan: spectral imaging and stellar occultation. A third type, that of measuring solar occultations, may also be periodically undertaken. Spectral imaging will be used to map and study trace gas and aerosol distributions, microphysical properties of aerosols, aurorae, lightning production and associated spectral/chemical characteristics, and, for Titan, surface mineralogy and topography. Stellar occultations by the atmospheres of Saturn and Titan and observed by VIMS will be used to study the vertical distribution of trace constituents (e.g. CH_4, C_2H_2 CO, and CO_2) and aerosols, particularly in Titan's stratosphere. Some thermal profile information may also be forthcoming from spectral regions where refraction is the primary extinction mechanism.

3.2.1. *Spectral Imaging—Spatial Distributions*

Measurements for atmospheres largely follow those for satellite surfaces, in that various combinations of spectral and spatial resolutions will be utilized, depending on the target-spacecraft distance. The actual combinations however are different, owing to the greater spectral activity in gases as compared to solids, the highest spectral resolution modes will be used most frequently.

Type A1: High-spectral-, high-spatial-resolution data sets acquired within 25 object radii. The full spectral/spatial resolution and spectral coverage of VIMS-VIS is utilized, as is the full (i.e. standard) spatial/spectral resolutions of VIMS-IR. The data may be limited to specific targeted regions (such as particular regions of belts and zones, storm systems, etc.). Multiple observations of these regions as a function of illumination and viewing geometry (i.e. center-to-limb observations as the feature rotates with respect to the spacecraft, and observations acquired at various phase angles) will enable the full three-dimensional character of the atmospheric region to be determined. For Saturn, such detailed sets of observations are referred to as *Feature Tracks* and *Feature Campaigns*. Specifically, a *Feature Track* is a set of center-to-limb observations acquired at one phase angle; A *Feature Campaign* comprises a set of *Feature Tracks*, obtained over the full range of available phase angles during one orbit. It is expected that at least one *Feature Campaign* will be acquired per orbit, comprised of at least five sets of *Feature Tracks*, with each *Feature Track* comprised of between three and seven individual *Type A1* observations, depending on the phase angle. In addition, a number of other *Feature Tracks* will be conducted per orbit, scrutinizing various other features for temporal variability and contextual relationship with primary *Feature Campaign* objects.

Some *Feature Tracks* are obtained at the same time that data for *Cylindrical Maps* are recorded. At these times large swaths of longitudes are mapped over a

relatively narrow range of latitudes. Other *Feature Tracks* are obtained in specific remote-sensing *Feature Track* observations in cooperation with other remote sensing instruments. These are typically accomplished at ranges less than seven Saturn radii (R_S), in order to provide the necessary spatial resolution needed by the full complement of remote-sensing instrumentation onboard *Cassini*. Still others are accomplished during VIMS-specific *feature tracks*.

In practice, it is also expected that many of the *Feature Track* observations will be acquired in cooperative "ride-along" mode with other remote sensing instruments. VIMS's ability to image a 32 × 32 mrad field of view allows coverage of a wide range of latitudes and longitudes, particularly when outside of 15 R_S, thus enabling many features to be captured within its field-of-view, even when spacecraft pointing is being directed at other places on Saturn by other instruments.

Feature Campaigns as done for Saturn will not be feasible for Titan, whose atmosphere is expected to rotate much more slowly than the 10-hr Saturnian period. The time when the spacecraft is within 25 Titan radii (R_T) is relatively short (i.e. typically 2.5–5.5 h), but *Feature Tracks* will still be possible due to the rapidly varying spacecraft-target geometry as *Cassini* flies over Titan. Approximately a dozen such *Feature Tracks* are expected per Titan encounter.

Type A2: High-spectral- and moderate-spatial-resolution data acquired outside of 25 object radii, utilizing the highest spectral/spatial resolutions of VIMS. At this range, global mosaics will be acquired wherein the target is covered pole-to-pole. For Saturn, these mosaics may be built up from full-disk imaging or from a set of pole-to-pole images acquired over a limited range of solar-illumination/viewing geometry, taking advantage of the relatively rapid rotation rate of Saturn to enable the acquisition of global mosaics under nearly uniform lighting conditions. For Titan, full-disk imaging will be the norm. At least one mosaic of Saturn will be acquired per orbit, lasting ten hours with a duty cycle of some 20%.

Type A3: VIMS-IR only observations for nighttime thermal measurements. These will be used particularly on Saturn to acquire high spatial-resolution maps when periapsis occurs on the night side, primarily to map out tropospheric distributions of trace constituents (e.g. PH_3, NH_3). In particular, *Cylindrical Maps* will be obtained wherein nadir views of Saturn's deep atmosphere will be acquired, peering through relative clearings in the clouds to deep-level "hot spots". Ten hours of continuous observations may be needed, depending on periapsis distance.

Type A4: VIMS-IR long-integration observations for weak emissions. Methane fluorescence will be observed on the dayside, and $H_3^+ Z$ emissions will be observed on the night side using this technique. Observations of high-altitude emissions are conducted within strong bands of atmospheric methane absorption. Integrations up to 10 s may be used.

Type A5: VIMS high-speed photometry mode for detection and characterization of lightning emissions. Under nighttime conditions, while relatively close to the planet (less than 10 R_S), VIMS stares at one location at a time, searching for lightning. When lightning strikes, the full spectrum is obtained, and acquiring data at

high rates (about 20 ms integrations), the chronological order of multiple lightning strikes in a single locale can, in principle, be ascertained. From analysis of the lightning emission spectrum in and out of methane absorption bands, it is hoped that the altitude of emission can be determined as well as the total energy for each lightning strike.

3.2.2. *Atmospheric Stellar Occultations*

Stellar occultations will be attempted periodically during Titan encounters, for a period of 5–10 min each. Integration times are typically 80 and 13 ms, respectively, for VIMS-VIS and VIMS-IR. These high sampling rates thus enable VIMS-VIS vertical resolutions of between 30 and 50 m for tangential spacecraft velocity components, relative to Titan, of 3–5 km/s. Observations last 3–6 min on average. Further details on particular occultation modes are discussed later.

3.3. RINGS

There are two major types of measurement objectives for the VIMS investigation with respect to Saturn's ring system: Spectral imaging and stellar occultation. Spectral imaging will be used to map and study the composition and mineralogy of Saturn's rings. Usually this will use *image*, *line*, or *point* instrument modes (see Section 5.2.1 for definitions). Stellar occultations by the rings and observed by VIMS will be used to study the dynamical structure of the rings. The *occultation* modes are used for these (see Section 5.2.2 where these modes are defined).

3.3.1. *Spectral Imaging of Rings*

The purpose of ring spectral imaging with VIMS is to determine the spatial distribution of various chemical species in Saturn's rings by mapping absorption bands in the visual and in the near infrared spectral regions. Radial mineralogical differentiation of the ring may be a key issue, related to ongoing transport phenomena in the rings, and related as well to the initial conditions through which the rings were formed (like a satellite breakup or the remnants of the protoplanetary nebula).

Another specific goal of VIMS is to characterize small-particle properties through the observation of the rings at various phase angles. Micrometer-sized particles are an important tracer of the ring dynamics because they are abundantly released during collisions, and also because they are sensitive to non-gravitational forces like radiation pressure or the Lorentz force. The visual and infrared channels of VIMS have access to the very wavelengths from which Mie scattering phase functions may be derived for these particles. Such functions yield some important physical properties of the particles (real and imaginary refractive index, size distribution).

Spectral identifications will require mapping the Saturnian ring system at the highest spectral and spatial resolution consistent with mission constraints. The best opportunity for spectral imaging of the rings occurs at Saturn Orbit Insertion when the spacecraft is closer to the rings than it will be for the rest of the Saturn Orbital

Tour. The present scenario calls for VIMS to be operated in line mode, using the shortest possible integration time consistent with useful signal precision (signal-to-noise ratio, or S/N). We note that VIMS-IR 2-D scan mirror is particularly convenient for that purpose since it allows us to choose the region of the ring which will be mapped, within the VIMS-IR 32 mrad field of view. During the rest of the orbital tour, ring regions to be mapped will be selected according to the orbit geometry, so as avoid redundancy and cover as much as possible of the ring system in the initial phases. In later phases, when interesting compositional and dynamical regions are discovered, they will be re-observed using a strategy specific to the phenomena being studied.

Some regions of dynamical interest will be mapped at the highest possible spatial resolution. In particular, spectral signatures near sharp edges, wave features, or narrow ringlets can provide evidence for the release of fresh material through enhanced collision rate. The radial width of the waves features is typically 100 km, i.e. barely resolvable by the VIMS instrument. Nevertheless, mineralogical differentiation near these regions can be detected, in particular during the close approach of the entrance orbit. On the other hand, the typical width of sharp edges is a few meters only. However, the streamline distortions near an edge are significant over radial distances of several tens of km. Thus, VIMS may detect and map mineralogical differentiation near edges also. Transient phenomena like clumps or braids in the narrow F ring will also be mapped by VIMS.

Depending on the precise orbital tour, VIMS observations of the rings will cover a complete range of phase angles, allowing the size range of small particles to be strongly constrained. The range of phase angles to be covered is 0–165°, the latter limit dictated by the need to keep direct sunlight off the VIMS focal plane.

Long exposures will also be made (consistent with the ∼1.2 s limit on the integration time in VIMS-IR) to map the structure and composition of faint rings like E ring, whose optical depth lies in the range 10^{-4}–10^{-5}. In addition, the comparison of the spectrum of Saturn's E ring to that of Enceladus will help to determine if Enceladus is indeed the source of the E-ring material as is presently thought.

3.3.2. *Stellar Occultations by Rings*

The purpose of ring-stellar-occultation observations with VIMS is to obtain high-S/N optical depth profiles of the rings, at a variety of longitudes, ring incidence angles, wavelengths and times during the *Cassini* orbital tour. The radial resolution is limited by the VIMS sampling time (13–100 ms, corresponding to 100 m–1 km typically), by Fresnel diffraction (typically 40 m, at 3-μm wavelength and a distance of 5 R_S), and by the diameter subtended by the stellar disk at the rings (10–100 m). The S/N achieved will depend on the sampling time, the stellar brightness, and the background flux of sunlight reflected by the rings into the VIMS aperture. Simultaneous observations at two or more wavelengths will permit this background signal to be subtracted from the stellar signal, once the

appropriate calibration data are obtained. Typical occultation durations will be 30 min–5 h, with 2 h a good average for a complete ring occultation near pericenter. A similar experiment may be done using the Sun as a source using the VIMS-IR solar port, but in this case the primary purpose is to quantify the ring extinction as a function of wavelength between 1 and 5 μm, at 300–1000 km spatial resolution.

During stellar occultations, VIMS will also obtain information on the ring particle size distribution by observing the 'aureole' of forward-scattered light surrounding the direct stellar line-of-sight. Utilizing the full VIMS wavelength range of 0.3–5 μm, and obtaining 32×32 mrad 'images', particle sizes between 2 μm and 3 mm can be probed.

Because the angular size of the effective VIMS pixel (0.5×0.5 mrad) is comparable to the pointing command and control errors expected for the *Cassini* spacecraft, an active method is necessary in order to keep the instrument bore-sighted on the star during a ring occultation. This will be achieved by using the VIMS-IR 2-D scanning capability to periodically perform small (4×4) raster scans, identify the location corresponding to the maximum stellar signal, and then reset the mirror position accordingly. Because portions of the rings are likely to be effectively opaque (notably the middle B Ring) this 'auto-guiding' function can be turned off for short periods according to a specified schedule.

In order to correct the ring occultation data for the presence of reflected ring light, a spatial map of the ring reflectivity spectrum is required. For this purpose, 1-D drift scans across the rings will be conducted at a range of phase angles and lighting conditions (lit side/unlit side, as well as various incidence angles), using the identical data mode used to take ring occultation data. For these scans, standard spacecraft attitude control will be sufficient. In fact, these scans may be identical to regular 1-D spectral maps of the rings acquired for other scientific purposes.

Full IR spectral observations of the occultation stars prior to the actual occultation observations will be necessary for calibration purposes, and for final selection of suitable occultation candidates. Some stellar observations must therefore be done during the interplanetary cruise phase, prior to SOI.

VIMS packets containing occultation data also contain absolute timing signals derived from the ultra-stable oscillator (USO) in the radio science subsystem. The exact relation between the photon-arrival time of the first data point in the packet and the recorded clock signal will be known to ± 1 VIMS sample, or 13 ms. The absolute precision of the timing signals will be maintained to the same level, or better, and the VIMS sampling rate will be controlled and known to an accuracy such that the maximum cumulative timing error over one packet is appreciably less than 13 ms. The overall goal is that the photon arrival time for any specified occultation datum can be reconstructed to $\pm$ 13 ms, after the data is received on the ground.

Ring occultations can only be carried out on inclined orbits, and are thus concentrated within certain limited periods of the baseline orbital tour. Only the ingress of the star behind the rings is observed, so as to permit acquisition of the star via

the star tracker prior to the occultation. Similar opportunities exist on most inclined ($i > 10^\circ$) orbits, and a great many more on the near-polar orbits in the last year of the baseline tour. A total of 50–100 stellar occultations by the rings may be observable during the nominal mission.

4. Instrument Description

This section presents a broad overview of the technical aspects of the VIMS instrument. For a detailed technical description, the reader is referred to the literature (Miller *et al.*, 1996; Reininger *et al.*, 1994) and *Cassini* project documents that describe the technical aspects of the VIMS instrument in detail. For a complete discussion of the operational aspects of the *Cassini* VIMS the reader is directed to the *VIMS Users Manual* (JPL document D-14200).

4.1. VIMS-VIS THE VISUAL CHANNEL

VIMS-VIS is a multispectral imager covering the spectral range from 0.30–1.05 μm. VIMS-VIS is equipped with a frame transfer CCD matrix detector on which spatial and spectral information is simultaneously stored. The CCD is passively cooled in the range (-20 to $+40\,^\circ$C. Radiation collected from VIMS-VIS telescope is focused onto the spectrometer slit. The slit image is spectrally dispersed by a diffraction grating and then imaged on the CCD: thus, on each CCD column a monochromatic image of the slit is recorded. On-chip summing of pixels allows implementation of a large number of operating modes for different observing conditions.

The maximum capabilities of VIMS-VIS are a spectral resolution of 1.46 nm and a spatial resolution of 167 μrad while in the high-resolution mode of operation. On-chip summing of five spectral $\times$ three spatial pixels enables the normal mode of operation whereby VIMS-VIS achieves a spectral resolution of 7.3 nm and a spatial resolution of 500 μrad. The total field of view of the instrument is $2.4^\circ \times 2.4^\circ$, although matching with VIMS-IR imposes the use of a $1.8^\circ \times 1.8^\circ$ FOV. The main characteristics of the instrument are listed in Table I.

As seen in the functional block diagram (Figure 1), VIMS-VIS is composed of two modules, the optical head and the electronic assemblies, housed in separate boxes. The VIMS-VIS optical head, shown in Figure 2, consists of two units: a scanning telescope and a grating spectrometer, joined at the telescope focal plane where the spectrometer entrance slit is located. The telescope mirrors are mounted on an optical bench that also holds the spectrometer. In fact, the optical bench is the reference plane for the whole instrument.

The telescope primary mirror is mounted on a scan unit that accomplishes two specific tasks: (a) pointing and (b) scanning. The scanning capability enables the 500 μrad IFOV of the nominal mode of operation by a two-step motion of the

TABLE I
VIMS-VIS System Characteristics (After Reininger *et al.,* 1994).

Spectral coverage	350–1050 nm
Spectral sampling (VIMS-VIS capability)	1.46 nm
Spectral sampling (*Cassini* requirements)	7.3 nm (5 pixel summing)
IFOV	0.17 × 0.17 mrad
Effective IFOV	0.5 × 0.5 mrad (3 × 3 pixel summing)
FOV (*Cassini* requirements)	1.83° × 1.83°
FOV (VIMS-VIS capability)	2.4° × 2.4°

primary mirror during each integration time; images are produced by scanning across the object target in the down track direction (push-broom technique). The pointing capability is used to image selected target regions in a range about 1.8° around the optical axis, and to observe the Sun, through the solar port, during in-flight radiometric calibration.

An in-flight calibration unit is located at the entrance of the telescope. The unit consists of: (a) two LEDs for a two-point calibration of the spectral dispersion and (b) a solar port for direct solar imaging and hence for radiometric calibration. Because the remote sensing pallet is body-mounted to the spacecraft, to image the Sun the spacecraft is reoriented to form a 20° angle with the boresight direction of the instrument and the instrument scan mirror needs to be moved to an angle of 4.8° from boresight. Under these conditions light from the Sun passes through a cutout

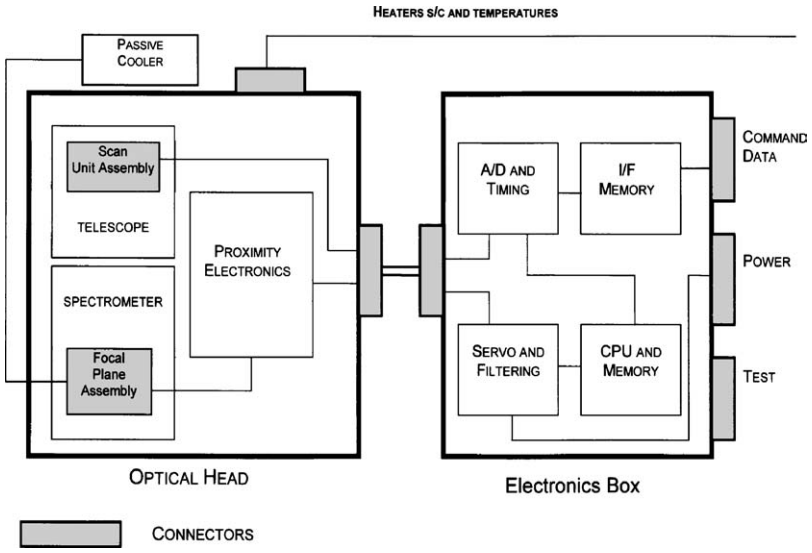

Figure 1. VIMS-VIS functional block diagram.

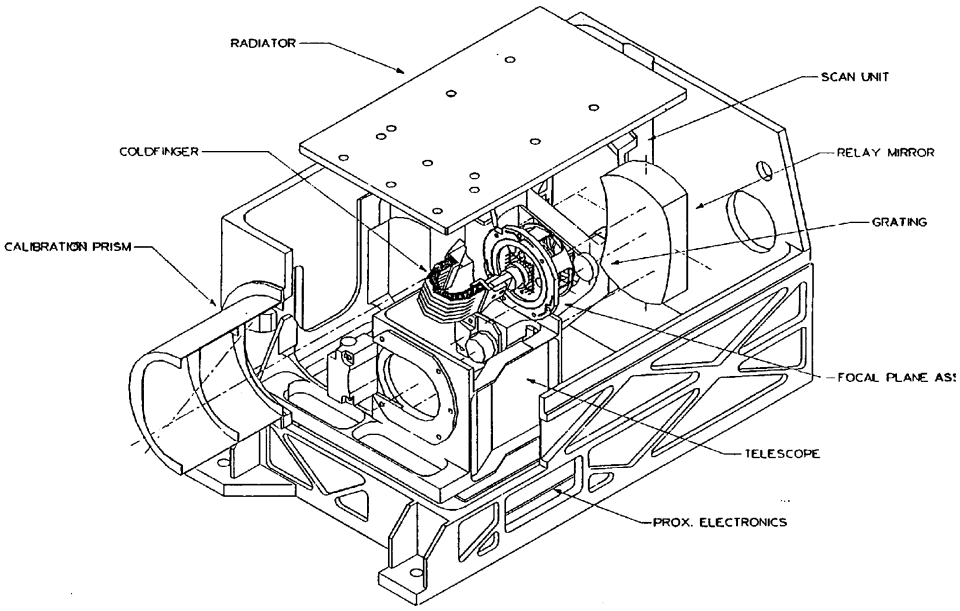

Figure 2. VIMS-VIS cutaway diagram.

in the instrument baffle and then through a prism that attenuates the solar radiation and redirects it towards the telescope primary mirror. Due to budget constraints, the high-resolution mode was been implemented and tested, but not calibrated. Calibration will be accomplished during the cruise phase to Saturn.

4.2. VIMS-IR THE INFRARED CHANNEL

In Figure 3 is a wire-frame drawing of VIMS-IR showing the major optical components along with the light paths. At the top of Figure 3 can be seen the visual channel with its light path and foreoptics, and near the bottom of Figure 3 is the infrared channel with its light path and foreoptics. Also shown at the right is the cover for the VIMS-IR optics that was successfully deployed as of August 15, 1999, some 50 h before the time of closest approach during the *Cassini* Earth Swingby. VIMS-VIS and VIMS-IR are mounted to a palette that holds them in optical alignment and helps to thermally isolate the instrument from the *Cassini* spacecraft. Thermal isolation is particularly important for the infrared channel because thermal background radiation from the IR spectrometer, combined with shot noise from leakage current in the InSb photodiodes of the 256 element linear array detector of VIMS-IR are the chief sources of noise in measurements obtained with the IR channel. The nominal operating temperature for the VIMS-IR focal plane is 55–60 K and for the IR foreoptics and spectrometer optics 120 K.

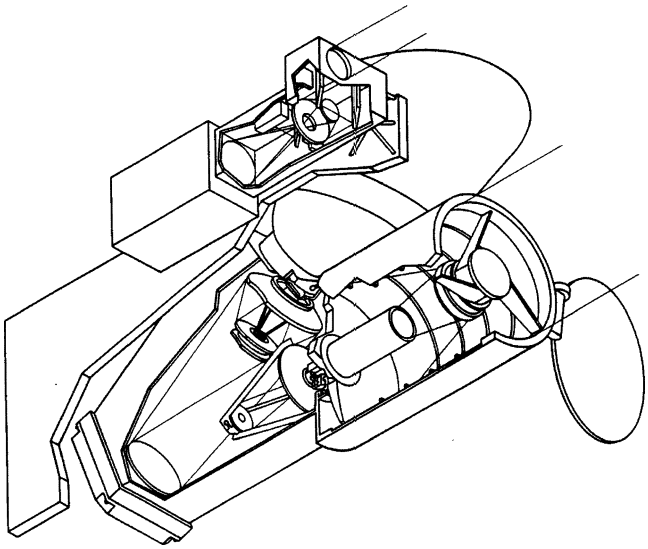

Figure 3. VIMS IR wire-frame drawing.

The VIMS instrument is mounted on the *Cassini* spacecraft by means of a palette (called the remote sensing palette or RSP) on which are also mounted the *Cassini* imaging science subsystem (ISS), the composite infrared spectrometer (CIRS), and the ultraviolet imaging spectrometer (UVIS). Mounting of all the *Cassini* remote sensing instruments on a common palette allows relatively precise boresight alignment of the four instruments, enhancing synergy between the four instruments.

Figures 4 and 5 are computer-aided design (CAD) models of the *Cassini* spacecraft with all of the major spacecraft components and their spatial relationship to the remote sensing palette indicated. Figure 4 specifically shows the mounting position and orientation of the VIMS instrument on *Cassini*. Figure 6 is a picture of the infrared channel very near the time that the VIMS instrument began its thermal vacuum and ground calibration tests prior to integration on the *Cassini* spacecraft. Also in Figure 6 are some of the nefarious characters that helped give birth to VIMS.

4.3. Functional Diagrams

Figure 7 is a functional block diagram of the entire VIMS instrument, with VIMS-VIS and VIMS-IR integrated on an optical pallet assembly (OPA).

4.4. Performance and Optical Specifications

4.4.1. *VIMS-VIS*

The optical specifications of both components of the VIMS instrument are given in Table II. The VIMS-VIS telescope is a *f*/3.2 system which uses a Shafer design to

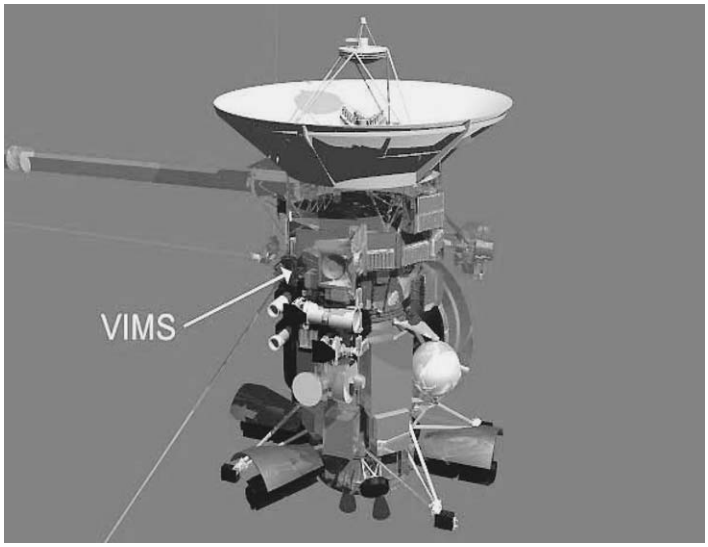

Figure 4. CAD model of *Cassini* orbiter with VIMS shown.

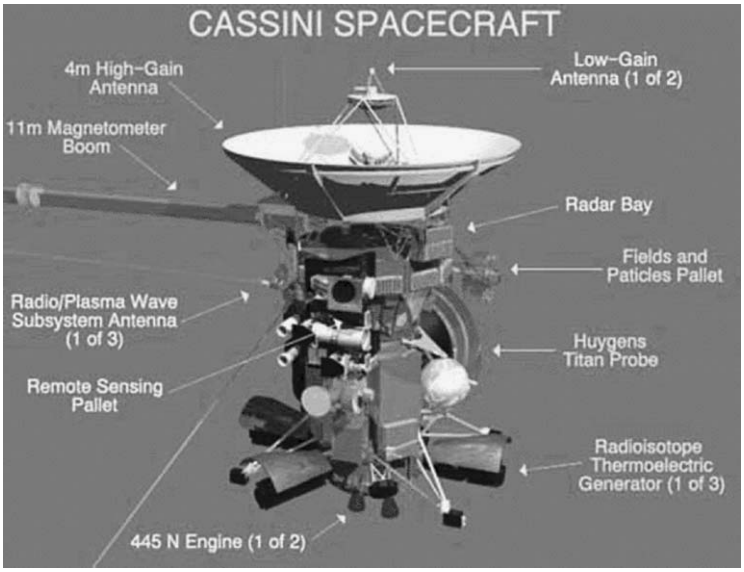

Figure 5. CAD model of *Cassini* with various subsystems indicated.

couple an inverted Burch telescope to an Offner relay system. The Burch telescope consists of a concave scanning primary mirror, a planar folding mirror, and a spherical convex secondary mirror. The Burch telescope produces a curved, anastigmatic virtual image which is fed to the Offner relay whose purpose is to produce a flat, real image on the telescope focal plane without loosing the anastigmatic quality

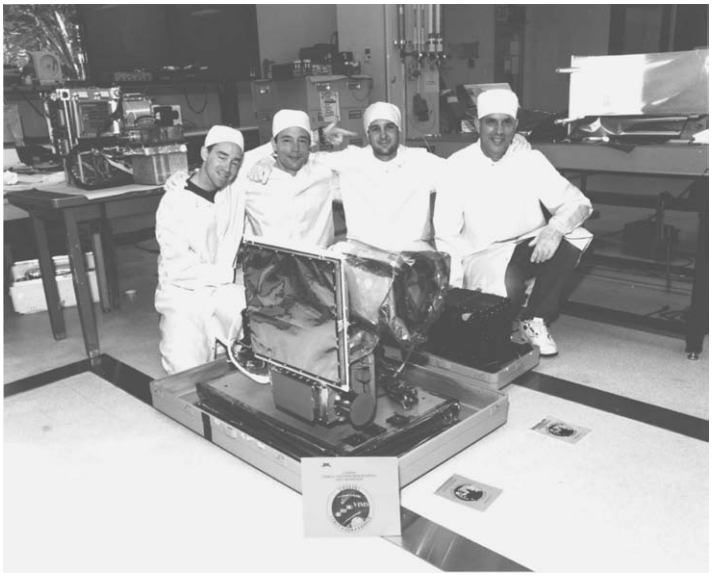

Figure 6. VIMS-IR and some of the engineers.

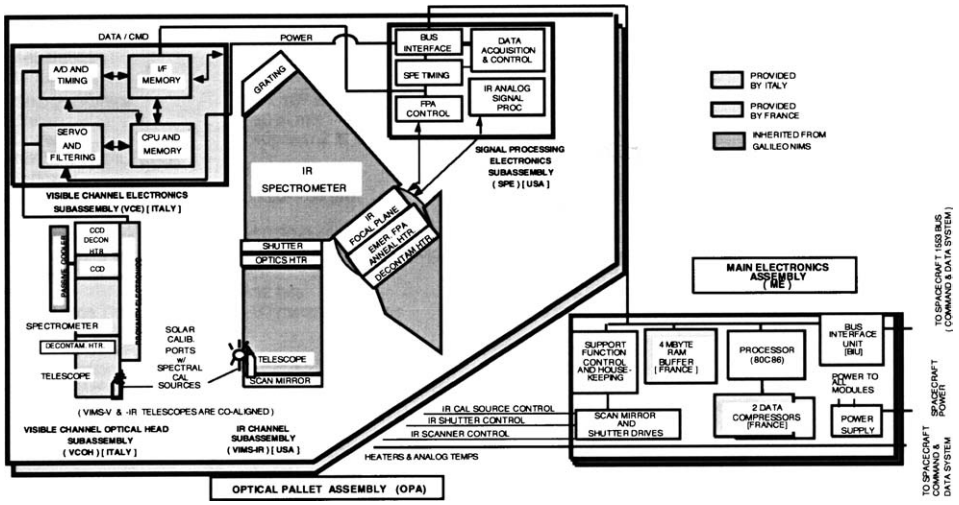

Figure 7. Integrated VIMS functional block diagram.

of the Burch telescope (See F. Reininger *et al*., 1994). The telescope is effectively diffraction limited at 0° scan angle over the full field, the encircled energy at 1.2° off-axis (maximum VIMS-VIS capability) is 97.8% for a 24 μm square (size of the CCD pixel); moreover, the geometrical spot sizes were under 12 μm at 0° scan angle over the full field.

TABLE II
VIMS-VIS and VIMS-IR optical system characteristics.

	VIMS-VIS VIMS-IR	Total system	
Spectral coverage	0.35–1.0 μm (0.3–1.0 μm by special command)	0.85–5.1 μm	0.35–5.1 μm or 0.3–5.1 μm
Spectral sampling	7.3 nm/spectal (96 bands) (1 × 5 sum)	16.6 nm/spectal (256 bands)	
Spatial characteristics			
Instantaneous field of view (IFOV)	0.17 × 0.17 mrad	0.25 × 0.5 mrad	
Effective IFOV	0.5 × 0.5 mrad (3 × 3 sum)	0.5 (0.5 mrad (1 × 2 sum)	0.5 × 0.5 mrad
Total field of view	64 × 64 pixels (32 × 32 mrad)	64 × 64 pixels (32 × 32 mrad)	32 × 32 mrad
Swath width	576 IFOVs (3 × 3 × (64)	128 IFOV (2 × 64)	32 mrad
Image size modes (fast scan)	1–64 pixels	1–64 pixels	1–64 pixels
Image size modes (slow scan)	1–64 pixels	1–64 pixels	1–64 pixels

The focal plane of the telescope is the entrance object plane of the spectrometer. The spectrometer is an Offner relay matched to the telescope relay (*f*/(3.2) that utilizes a holographically recorded convex spherical diffraction grating as the secondary mirror of the Offner relay. The grooves of the grating have a rectangular profile. In addition, two different groove depths are used in adjacent sections of the grating to enhance the grating efficiency spectrum in the UV and IR regions. This compensates for the spectral response function of the CCD detector (quantum efficiency) and for the solar radiance (the peaks occur at about 675 and 475 nm, respectively). In 67.5% of the grating surface, there is a groove depth of 300 nm while the remaining 32.5% is covered with grooves of depth 440 nm. The spectrometer spot diagrams show that for a 0° scan angle all the energy falls inside a CCD pixel over the full angular and spectral fields.

The CCD detector is a 512×512 Loral frame-transfer, front-side-illuminated device. The pixel size is 24 μm $\times$ 24 μm. Half of the detector is used for the frame transfer, and the effective sensitive area corresponds to a 256 spatial $\times$ 480 spectral pixels. To minimize second- and third-order light from the grating, two long-pass filters were deposited on a window used to seal the detector. The junction between the two filters (located at 601 nm) induces a dead zone on the detector of less than 40 μm (a nominal spectral pixel is 120 μm wide). To improve CCD detector responsivity in the UV region of the spectrum a Lumigen coating has been deposited on the CCD sensitive surface in the region 300–490 nm.

The performance of the instrument can be evaluated by its S/N for a given configuration of the instrument and for a given target scenario. VIMS-VIS has been designed to guarantee a S/N $>$ 100 under all observing conditions for the nominal mode of operation.

4.4.2. *VIMS-IR*

The VIMS infrared channel optical design follows that of the Galileo NIMS instrument, but incorporates several improvements that result in much better performance than that of its predecessor. The IR foreoptics is a 23-cm diameter Ritchey Cretien telescope operating at $f/3.5$. It is equipped with a secondary mirror that can be scanned in two orthogonal directions, resulting in the scanning of 64×64 mrad scene across a 0.2×0.4 mm entrance slit. The entrance slit is coupled to a classical grating spectrometer using a *f*/3.5 Dahl-Kirkham collimator. The spectrometer incorporates a triply-blazed grating whose blaze angles have been adjusted so as to compensate for the steep drop in intensity of the solar spectrum toward long wavelengths, thus resulting in a more uniform signal-to-noise ratio across the 0.85–5.0 μm wavelength region when viewing spectrally neutral objects in sunlight. The dispersed light from the grating is imaged onto a 1×256 array of InSb detectors using a $f/1.8$, all reflective, flat-field camera. The IR detector employs four filters, used both for order sorting and for blocking excess thermal radiation from the spectrometer optics. The secondary mirror of the VIMS foreoptics is articulated using a two-dimensional, voice-coil actuator capable of 0.25

mrad steps in the fast-scan direction and 0.5 mrad steps in the slow-scan direction. Because the optical performance and design of NIMS have been described in detail elsewhere (Aptaker, 1982; Macenka, 1982), we direct the interested reader to those discussions. Below we will focus in more detail on the optical improvements to the NIMS design.

The major areas in which the VIMS design improves on the NIMS design are: a two-axis, voice coil actuator for articulation of the telescope secondary mirror; a fixed, three-blaze grating; an improved shutter to replace the NIMS focal-plane chopper; on-board solar and spectral calibration; and an improved IR detector.

The two-axis scan mechanism employs four voice coil actuators for articulation and two linear variable displacement transformers for position sensing. The secondary mirror is mounted on a monolithic gimble ring supported by four flexures. The flexure life is predicted to be greater than 20 million cycles. The range of motion is 128 steps in the fast-scan direction and 64 steps in the slow-scan direction, both covering approximately 64 mrad in angular displacement. The step transition time is a maximum of 5 ms.

The grating is blazed in three separate zones designed to more evenly distribute the performance of the spectrometer over the large 0.85–5.1 μm spectral region covered by the VIMS instrument. The groove spacing is 27.661/mm, and the first, second and third blazes cover 20, 40 and 40%, respectively of the area of the grating. The three zones are blazed at wavelengths of 1.3, 3.25 and 4.25 μm, respectively.

The shutter mechanism of VIMS is a blade located just in front of the spectrometer slit. The shutter can be commanded to block the light from the foreoptics, thus allowing a specific measurement of the thermal background radiation and detector dark current that collects during a given integration period. In normal operation this is accomplished at the end of every fast scan, and the result is both subtracted from the open-shutter measurements, and downlinked with the data. A LED-photosensor pair is employed to detect blade position. Lifetime tests indicate a minimum life of 7×10^6 cycles at the normal operating temperatures of 120–140 K.

The IR focal plane assembly is a linear array of 256 InSb photo detectors read by two FET multiplexers. Each detector is 200×103 μm in size and positioned on 123 μm centers. Each multiplexer handles 128 detectors, and the two multiplexers are interdigitated; thus, each reads every other detector along the array. This arrangement was chosen to prevent the loss of half of the spectral range of the instrument if one of the multiplexers fails. The detector is housed in a Kovar package, specially constructed to mimic the dimensions of the NIMS detector, and to allow the employment of most of the original design of the NIMS passive cooler. To keep the detector dark current within the range necessary for observations at Saturn, the detector must be cooled to 60 K or less, and becomes non-operational for science observations at 77 K. Mounted in the Kovar package and over the detector array are four order-sorting filters that also reduce the amount of stray thermal radiation from the spectrometer optics incident on the detectors. The filters are arranged in four

contiguous segments, the lengths of which were carefully chosen so as to provide efficient order sorting and to place the slight gaps between the filters in places that would not have an adverse impact on science observations in the Saturn system. For more details on the filters (or on any of the above topics) the reader is referred to Miller *et al*. (1996).

The final two enhancements to the NIMS design are the addition of a port through which the Sun can be observed and a laser diode that is used for onboard wavelength calibration. Detailed descriptions of the solar port and the on-board spectral-calibration capability of VIMS appear later in this document.

4.5. Data Handling, Compression, and Buffering

Reversible data compression for the VIMS instrument is performed by a dedicated module based on a digital signal processor working at 6 MHz that interfaces with the VIMS command and data processing unit through an input first-in-first-out buffer and an output first-in-first-out buffer. The data compression algorithm consists of a preprocessing routine and a Rice entropy encoder (Rice *et al*., 1991). The data unit for compression is a series of 64 spectra (a slice) obtained during one scan (i.e, in nominal 64 $\times$ 64 image mode or 64 $\times$ 1 line mode) or a series of scans. This provides 64 pixels each with 352 spectels. Each slice is divided into 11 sub-slices of 32 spectels (three for the visual channel and eight for the IR channel), and each sub-slice is compressed independently. This restricts the impact of possible bit errors either in random access memory (single event upsets) or during transmission.

The preprocessing routine for the 64 pixel $\times$ 32 spectel sub-slice is based on the large entropy content of variations in lighting and albedo when compared to spectral signatures (more than 5 to 1). Four evenly distributed channels are summed and divided by four so as to obtain a representative "brightness line" for this spectral range. This line and the brightest spectrum are differenced, then Rice encoded into a header. The matrix product of the brightest spectrum by the brightness line provides a model rectangle where every pixel has the same brightness as the actual data and the same spectrum as the brightest pixel. The model rectangle is then subtracted from the actual data. The entropy of the resulting "spectral rectangle" is directly related to the variations in relative spectral characteristics. It is then differenced along the spatial direction and the 63 $\times$ 32 differences are Rice encoded. Reconstitution on the ground first recovers the brightness line and brightest spectrum from the header, then the rectangle of 63 $\times$ 32 differences, and finally the original data taking advantage of the fact that model and data are identical for the brightest spectrum. The compression ratio for fully reversible compression ranges between 2 and 3 depending on the actual entropy of the data.

Reversible compression is highly sensitive to over sampling of the noise. Each doubling of the data number (DN) level of the noise adds 1 bit per data element to the compressed string. After calibration, the shot noise can

be accurately predicted from the data itself. The algorithm provides the possibility of defining two DN limits, Lim2 and Lim4, above which the total noise is expected to exceed 2 (4) DN. Each datum in the spectral rectangle is divided by 2 if the model value exceeds Lim1 (Lim2) (4). The quantization noise after reconstitution is then 2 × 0.28 DN (4 × 0.28 DN) instead of 0.28 DN hence the compression algorithm is able to automatically divide the actual gain by 2 (4) for DN levels associated with large shot noise. Setting Lim1 and Lim2 to 4096 (larger than any 12 bit data) provides fully reversible compression.

A data buffer of 4 Mb is used for buffering data between the VIMS processor and the spacecraft. Its full memory is divided into two redundant pages of 2 Mb, each consisting in 32 sectors organized as a matrix of four lines by eight columns. Each sector contains two 32K × 8 RAM chips, connected in parallel to achieve a 16-bit architecture. Each sector can be specifically selected. The transfer is made via a direct memory access (DMA), with write and read maximum times of 240 and 140 ns, respectively. Each column includes an "anti-latchup" capability and over-current protection, which switches off the power autonomously in case of over-threshold current (100 mA in 11 μs or 200 mA in 4.4 μs).

Dassault Electronique of France developed the VIMS data buffer. It was qualified for radiation levels up to 20 krad, storage temperatures of ($-55\,^{\circ}$C, $+125\,^{\circ}$C, and operating (full functional) temperatures of ($-40\,^{\circ}$C, $+80\,^{\circ}$C. It consists of a single board, with one page on each side, 162 × 129 × 17 mm^3 in size, and 625 g in mass. With a 5 ± 0.25 V supply voltage, its power consumption is 1.5 W in stand-by mode, and 2 W during operations.

5. Instrument Operation

5.1. General Operational Considerations

5.1.1. *VIMS-VIS*

VIMS-VIS operates in different operating states and in different modes. The CCD data acquisition mechanism combines pixels by summing them on chip, both in the spatial direction (along slit) and in spectral direction. The use of a scanning secondary mirror allows summation of pixels parallel to the slit. Thus square spatial pixels are generated in lower spatial resolution modes. There are five operating states of the instrument as a whole: science status, internal calibration, uploading, downloading, and off. The scientific data and the internal calibration data are in turn defined by different operating parameters that translate the scientific requirements for the data collection into the physical, electrical and optical characteristics of the instrument.

When VIMS-VIS is switched on it goes into the science state in the nominal mode. The commands to change the operating state are sent to the VIMS-VIS electronics together with the set of parameters relevant to define a new state. The scientific data set can be obtained in different "operative modes" according to the

different observation scenarios. For each mode the operating parameters define the characteristics of the data to be collected, such as spatial resolution, spectral resolution, and extent and location of the scene to be observed in the instrument FOVs. When the instrument is switched on, the combination of different parameters that define the different observation modes are loaded. The input parameters of the scientific data acquisition modes are:

(a) Summing parameters,
(b) Swath width,
(c) Swath offset,
(d) Spectral offset,
(e) Swath length,
(f) Exposure time,
(g) Exposure time delay,
(h) Mirror,
(i) Gain,
(j) Anti-blooming.

Different combinations of these parameters lead to several different operative modes.

5.1.2. *VIMS-IR*

The two main considerations in the design of the IR component of VIMS are flexibility and compatibility with the other *Cassini* remote sensing instruments. A range of programmable parameters, including integration time, swath width and length, and mirror position enable the instrument to adapt to a variety of observing modes dictated by the scientific objectives of each phase of the *Cassini* mission, and by synergistic observations with other *Cassini* instruments. Software enhancements uploaded after launch provide more levels of flexibility, including spectral editing, additional image sizes, increased spectral resolution in the visual channel, and a doubling of the instrument's spatial resolution.

5.2. Specific Operational Modes

Image, *line*, *point*, and *occultation* are instrumental modes of operation. An operational mode corresponds to specific instrumental parameter settings, as was illustrated in Section 5.1.1. The *image*, *line*, and *point* modes are the most frequently used. Observation types (Sections 3.1.1. and 3.2.1) are use oriented variations on single modes.

5.2.1. *Image, line* and *point* mode descriptions

The majority of scientific observations by VIMS will be in the *image*, *line*, or *point* modes. Several modes were tested for a variety of integration times and instrument gain states. For image sizes smaller than 64×64, the scan mirror can be offset from the boresight in both the x and z directions. In the *image* mode, VIMS is a framing

instrument, producing a spectral cube of 352 images in the specified size. Three routinely used sizes for the images are a full 64 × 64 IFOVs, 12 × 12 IFOVs and a single (1 × 1) IFOV. The 12 × 12 image size corresponds to the field of view of the image science subsystem's narrow angle camera (ISS NAC). This mode will be used to efficiently gather data simultaneously with ISS. The 1 × 1 image size corresponds to *point* mode, which will be used primarily for stellar occultations or for the accumulation of spectra during a rapid flyby of a target for which motion compensation is not possible. Rectangular combinations of 12, 32, and 64 are also in the group of tested modes: these will be used during periods when the data rates or volume is constrained. It is possible to offset the position of the scan mirror so that "sub images" are gathered in a position offset from the center of the field of view. Compositional mapping and photometric studies of Saturn, the surfaces of the icy satellites, Titan, and the rings, and dynamical studies of Saturn and Titan will be performed primarily in the image modes.

The VIMS instrument was also designed to obtain data in single lines of either 12 or 64 IFOVs parallel to either the spacecraft's *x*- or *z*-direction. The line mode parallel to the *z*-direction will be used in synergistic studies such as atmospheric profiles of Saturn and Titan with CIRS and UVIS, both of which have slits parallel to this axis. *Line* mode can also be operated such that the spacecraft's motion scans a second spatial dimension. These modes of operation are useful, for example, in a rapid flyby where motion compensation is not possible.

5.2.2. *Occultation Modes*

VIMS is the only instrument on the *Cassini* payload capable of observing stellar occultations in the visual and near IR portion of the spectrum. Stellar occultations by the atmospheres of Titan and Saturn will be used to derive the vertical distribution and microphysical properties of aerosols, and the stratospheric temperature profiles of these two bodies. Stellar occultations of the rings of Saturn will provide a sensitive probe of their radial structure, optical depth, composition and physical properties.

Occultations will be executed in the point mode. Before each occultation a 12 × 12 image of the star will be obtained. On-board software will seek the pixel with the maximum brightness. The instrument's mirror will be offset so that data is gathered in this pixel. If necessary, additional images can be gathered during long occultations to check that the star is still centered in the selected pixel. If the star has drifted, the mirror can be repositioned so that data are gathered from the pixel with the maximum brightness.

Three different modes of ring occultation observation are currently envisaged, with different data rates and spectral coverages:

Occultation mode 1: In this mode, which is applicable to stellar occultations by Saturn, Titan, and the rings, complete IR spectra are recorded, compressed, and either stored in the VIMS internal buffer or in the spacecraft on-board solid state recorder (SSR). The scan mirror oscillates so as to synthesize an effective 0.5-mrad square pixel for each spectrum. The sampling rate is adjusted, up to a maximum of

$\sim$10 Hz (one complete spectrum every 0.1 s). The maximum data rate (2:1 compressed) is 0.5 $\times$ (256 channels $\times$ 12 bit (10 Hz) = 15.4 kb/s. Typical data volumes are 5 Mb for a 300-s atmospheric occultation, and 110 Mb for a 2-h ring occultation. A modification of this mode, employed for the aureole observations, is to interrupt the regular occultation data stream with a full 64 $\times$ 64 pixel spatial/spectral map of the starlight scattered by the rings into the instrument FOV. Such a map would require 8.6 Mb of data, compressed, and take $\sim$450 s at 100 ms sampling. Since each pixel subtends at least 150 km on the rings at 5 R_S, the full image covers a patch about 9600 km square, about twice the distance the star travels across the rings in 450 s, and comparable to the largest homogeneous regions in the A, B and C rings.

Occultation Mode O2: In this mode, to be used primarily for ring occultations (but possibly also for icy satellite occultations), edited spectral averages are returned at the maximum VIMS sample rate of 77 Hz. Using spectral editing mode, a small number of spectral editing masks will be chosen, but a typical mask would require the co-addition of 15–30 contiguous spectral channels centered at four different wavelengths. A typical example might be 30 co-added channels centered at 2.00, 2.25, 2.90, and 3.50 μm. As in *mode O1*, the internal mirror oscillates every 6.5 ms to synthesize a 0.5 mrad square pixel. The four co-added signals are stored or transmitted, uncompressed, every 13 ms, for a data rate of four channels $\times$ 12 bit $\times$ 77 Hz = 3.7 kb/s, plus timing and housekeeping data. Total data volume is 27 Mb for a 2-h occultation.

Occultation Mode O3: Solar occultations. During a solar occultation experiment VIMS stares at the Sun through its solar calibration port, monitoring the extinction of sunlight by Saturn's rings, Saturn's atmosphere or Titan's atmosphere. Because the Sun has a large angular diameter even at Saturn's distance, (0.9 mrad at 10 AU), the maximum spatial resolution under these conditions is 300 km, and the necessary sampling time about 15 s or longer. Typical observations of the rings, for example, would result in full IR spectra every 15 s, for one spatial pixel, yielding a data rate (compressed) of 102 bps and a data volume of 740 kb for a 2-h occultation.

5.2.3. *Solar Port*

The solar port of VIMS was added late in the instrument design stage to recover some of the capability lost by the deletion of the *Cassini* spacecraft's calibration target. As a bonus, the solar port is capable of performing observations of solar occultations for atmospheric and ring studies.

The solar port strongly attenuates the solar spectrum that, once it passes through the solar port itself, follows the same path through the instrument as photons incident on the boresight. Its chief purpose is to acquire a solar spectrum that can be used to remove the effects of solar illumination from the VIMS data to obtain accurate scales of relative and absolute reflectance. The port's boresight is offset from VIMS main optical axis by 20 $^\circ$, to coincide with the optical axis of the UVIS instrument.

This configuration facilitates compatible operations between the two instruments for solar occultations of the atmospheres of Titan, Saturn, and of the rings.

The large attenuation factor is achieved by the small aperture of the solar port in comparison to the main beam, and by a series of one 70° and 90° reflections from right angle prisms made of ZnSe. Most of the incident flux is reflected back out of the entrance aperture by internal reflection in the prisms. The beam exiting the cal port is first focused by the primary and secondary telescope mirrors onto the VIMS-IR entrance slit, and then it enters the spectrometer. The incident solar radiation will illuminate only a small portion of the diffraction grating, because the cal port aperture samples only a portion of the main instrument's aperture. The optical design ensures that this region overlaps the short and medium-wavelength blaze regions on the grating, in the ratio of 1:3. The long-wavelength blaze is not illuminated. The predicted attenuation factor is 1.35×10^{-4} at 0.85 μm, 1.09×10^{-4} at 3.0 μm, and 1.04×10^{-4} at 5.0 μm. The actual attenuation factor in flight, measured by observing the Earth's moon in both the occultation port and the main aperture, is about 2.5×10^{-6}.

5.2.4. *IR and VIS Timing and Coordination*

Although the infrared and visual channels have separate optics and detectors, the two data streams are combined in the instrument's electronics so that a single spectrum of the same physical area on the target is produced. The visual channel utilizes an area array so it is able to gather an entire line of data during a single integration. The same line synch pulse that initiates the IR scan synchronizes the acquisition of the visual line. After the first visual integration period is complete, the entire frame of data is transferred and stored within the CCD for initial processing. The line of visual data is then sequentially read out and digitized by the visual channel electronics. Three lines of visual data are accumulated during the time of the forward scan of the IR channel. These individual visual pixel elements are then summed three by five (both spatially and spectrally) to yield a line of square pixel elements of ~0.5 mrad and with spectral channel widths of ~7 nm. This line of visual data is transferred to the instrument's main electronics over the global bus in exactly the same fashion as the IR data. The integrated visual and infrared spectra are then stored in the control processor's RAM.

6. Instrument Calibration and Cruise Data Analysis

6.1. Synopsis of the Ground Calibration

Spectral calibration of VIMS occurred in three separate steps. As above, we denote the visible spectral region component (channel) of VIMS as VIMS-VIS, and the infrared component (channel) as VIMS-IR. VIMS-VIS was calibrated separately in Italy prior to integration with VIMS-IR at JPL. VIMS-IR was calibrated in the thermal vacuum tests at JPL January 28–February 5, 1996. The integrated

instrument was further tested at the JPL thermal vacuum facility July 16–17, 1996. This final test only included filter transmission and mineral target tests.

The spectral calibration resulted in a specification of the wavelength position and bandpass of each VIMS spectral channel across the instrument field of view and as a function of temperature. The VIMS-IR spectral response is identical across the full field of view to within about a nanometer (nm) over the temperature range tested. The VIMS-IR sampling interval is about 16 nm in the IR, thus a 1-nm shift is a small fraction ($<7\%$) of the sampling interval. VIMS-VIS has a sampling interval of $\sim$7 nm and tests show stability to better than about 0.3 nm.

The detailed plan for the VIMS ground calibration evolved over a period of approximately four years, being completed in mid-1995, roughly six months before the actual measurements were to commence. The time frame for the ground calibration was driven by the planned delivery date of the fully integrated VIMS instrument in the September–October period, 1996. As mentioned above, because VIMS-VIS was not completed at the time of the main calibration, only VIMS-IR was calibrated. As a result of the slip in the schedule for he delivery of VIMS-VIS, a substantial recalibration of the integrated instrument has been undertaken while Cassini is in route to Saturn. The details of the efforts to calibrate the VIMS instrument in flight appear later in this document.

The main ground calibration of the IR channel was carried out in six separate areas: radiometric/flat field response, geometric, polarimetric, spectral, and solar port response. In the early phases of the genesis of the VIMS ground calibration plan, measurement of VIMS stray light rejection performance was also envisioned, but practical difficulties in performing those measurements under vacuum and at the operational temperatures required necessitated elimination of the groundbased measurements in favor of measurements in flight. Those measurements are discussed later in this document.

The actual measurements were carried out in the JPL thermal vacuum testing facility in the largest thermal vacuum tank available. The in-flight thermal environment for VIMS was simulated by cooling the interior surfaces of the thermal vacuum tank with liquid N_2, and providing a cold target that filled the fields of view of the passive coolers of both VIMS-VIS and VIMS-IR with a high-emissivity surface cooled to 4 K. In retrospect, the thermal environment of the JPL thermal vacuum tank and the cold target was quite accurate because the temperatures of the instruments optics and focal planes in flight are within a few K of those measured while the instrument was in the test environment.

6.2. Radiometric Calibration

6.2.1. *VIMS-IR*

The radiometric response of VIMS-IR was carried out before launch in the thermal vacuum facility at the Jet Propulsion Laboratory. A team of scientists, supported by the instrument engineering team at JPL, designed and carried out these

measurements. The team members responsible are Thomas B. McCord (lead), Robert Brown, Angioletta Coradini, Vittorio Formisano, and Ralf Jaumann. Also contributing were Giancarlo Bellucci, Bonnie Buratti, Frank Trauthan, Charles Hibbitts and Gary Hansen. Two sessions were conducted, one in January and the other in July of 1996. In-flight calibration efforts were conducted during the Venus, Earth and Jupiter flybys, and for two star observations. A workshop was held in Hawaii in February 2001 to review the information obtained. Additional people contributing post launch were Kevin Baines, Roger Clark, and Robert Nelson.

The equipment facility during the ground calibration included a JPL thermal vacuum chamber cooled by liquid nitrogen and containing the instrument, which viewed the outside through a window with known optical transmission. A reflecting collimator fed light from several sources to the instrument. The calibrated sources were a glow bar and a tungsten lamp; their energy delivered to the instrument was controlled by adjustable iris diaphragms at the exit of the lamps. The light sources and delivery system were covered to eliminate outside light and, during the first session, the tent was purged with dry nitrogen to reduce the effects of the atmosphere gas absorptions (mainly CO2 and H2O). Measurements were made at several instrument and focal plane temperatures, but most measurements were made with the focal plane temperature in the range 60.7–61.69 K. Data were acquired at several light levels and integration times, including zero.

The characteristics of the instrument that were explored were dark current (detector thermal carrier generation and electronic off-sets), background signal (mostly thermal radiation from the chamber window and from outside), linearity of response, ratio of responses at the two gain states, performance of the detector for two different bias levels, and overall radiometric response over the spectral range. The instrument was determined to be linear within the measurement error to detector saturation. The dark current, background, gain ratios and behavior at different bias are reasonable, stable and as expected. The overall spectral responsivity was most difficult to calibrate due to several factors, including an unexpected and unknown (at the time) change in a light source during the calibration effort. This effort has been enhanced during in-flight calibration efforts and the responsivity calibration is converging.

In-flight calibrations were conducted at Venus only for the visual channel because the cooler cover was not yet removed from the IR channel radiator. The entire instrument calibration was tested at the Earth–Moon (for the Moon only) and the Jupiter fly-bys and for two star observations. The data are still being analyzed at this writing for the in-flight calibrations, but the general result so far is to further refine the calibrations and to gain better understanding of the instrument performance, which remains as expected.

One interesting characteristic experienced is the difficulty of achieving precise and stable calibration for sources smaller than the spectrometer slit width (sub-pixel sources). This is because the effective spectral resolution of the spectrometer and the exact location of the source image on the detectors depend on the size of the

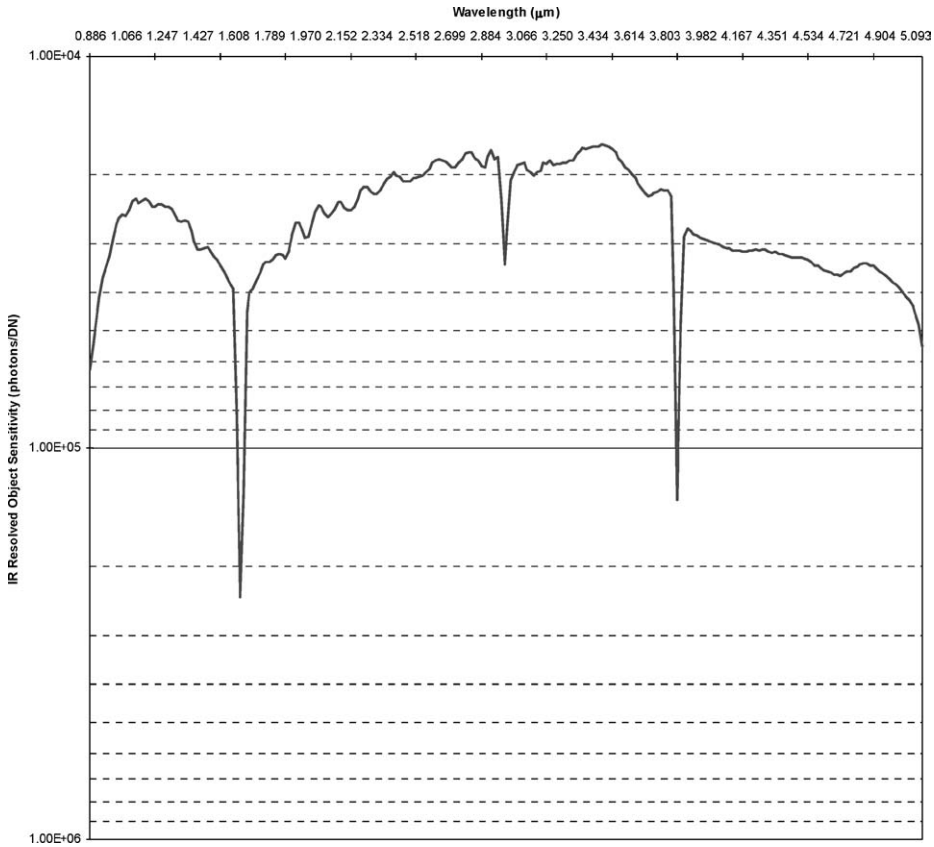

Figure 8. Spectro-radiometric response of the VIMS-IR channel as a function of wavelength in photons per data number. This plot represents the status of the calibration as of the writing of this article. Improvements and changes are expected with time and further analysis.

source and its exact location in the focal plane. Thus, it will be difficult to precisely predict radiometric performance for sub-pixel sources. Nevertheless, for sources that fill the slit, the instrument behavior is normal and as expected.

The spectro-radiometric response function as currently known is given in Figure 8. Improvements and changes are expected with time and more analysis. Thus, the reader is referred to the VIMS planetary data system (PDS) archive for appropriate calibrations to be used with flight data.

6.2.2. *VIMS-VIS*

VIMS-VIS was constructed and calibrated in Italy, at Officine Galileo. It was calibrated in two phases: (1) at Officine Galileo prior to the integration with VIMS-IR, and (2) at JPL after the integration on the remote sensing palette. The activity carried out at JPL was mainly devoted to geometric measurements, that is, co-alignment of the two channels and measurement of the relative radiometric response.

Furthermore, the instrument spatial response (measurement of the image quality through the instrument modulation transfer function and point spread function) was evaluated as part of the full functional tests performed at Officine Galileo prior to the calibration activity.

VIMS-VIS was placed inside a vacuum chamber equipped with a thermally stabilized radiator connected to the CCD and capable of keeping the CCD at a temperature in the range -20 to $40\,^{\circ}$C under a residual pressure $<10^{-4}$ mbar. The chamber has a window made of TVC, with transparency better than 0.9 throughout the entire spectral range. VIMS-VIS was mounted on two computer-controlled rotating tables for fine positioning at a range of azimuthal and elevation angles. Two lamps were used to cover the full spectral range: a xenon lamp for the range 0.3–0.4 μm, and a tungsten lamp between 0.4 and 1.035 μm. The lamp with its housing, which includes a condenser and a diffusing screen to improve light uniformity, was positioned at the input slit of a Jobin-Yvon HR640 monochromator capable of better than 0.05-nm resolution (band width at half height) over the VIMS-VIS spectral range. The monochromator output was then used to illuminate a slit, pinhole or test targets (corresponding to a specific type of test) placed at the focus of an off-axis collimator. The collimated beam was fed to the instrument inside the vacuum chamber. Unfortunately, the collimated beam had an unknown spectral irradiance; thus, we had to devise a method to measure it. This was achieved using a beam splitter of known optical properties, placed in the optical path at $45\,^{\circ}$ in front of the chamber window. The reflected portion of the beam was collected by a calibrated photodiode to monitor the irradiance output of the light source. An additional calibrated photodiode was placed every 50 nm (or 50 monochromator steps) directly in front of the collimator to have direct calibration at the collimator aperture.

Only one-sixth of the full VIMS-VIS FOV could be instantaneously illuminated with the available collimator, thus a time consuming procedure was implemented to repeat a full spectral sweep (0.3–1.05 μm in 1 nm steps) to cover the field of view of the instrument.

The radiometric calibration of VIMS-VIS was as follows. The unit response (UR) of the instrument is defined as the output in data numbers (DN) when the instrument entrance pupil is fed with a light beam of 1 W cm^{-2}, and this beam is collected entirely into a single spectel and into a unit solid angle, for an integration time of 1 s. This quantity was directly measured along with its dependence on wavelength. The spectral calibration was performed in order to evaluate the spectrally weighted center of each channel as well as the spectral width. The spectral width of each spectel is 7.33 nm. For a detailed discussion on the calibration see Capaccioni *et al.* (1998).

We note that the radiometric transfer function obtained at Officine Galileo during on ground calibration of VIMS-VIS when applied to the Moon and Venus illuminated side is insufficient to remove instrumental effects. Moreover two problems are apparent: a shift in wavelengths of about two nominal pixels and an inadequate

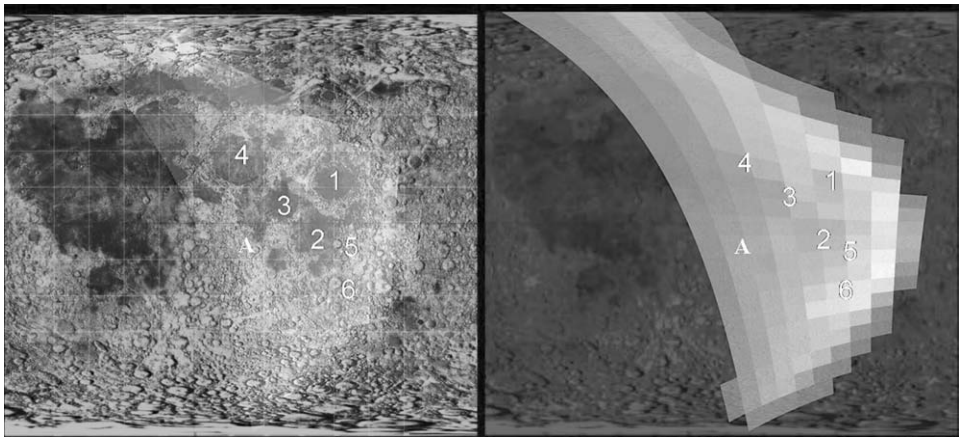

Figure 9. The VIMS-VIS field of view on the Moon during the flyby of August 18, 1999. Key: 1 Mare Crisium, 2 Mare Fecunditatis, 3 Mare Tranquillitatis, 4 Mare Serenitatis, 5 Langrenus, 6 Petavius, A Apollo 16 landing site.

removal of instrumental effects, particularly at short wavelengths. So we measured a new unit response function using the Venus and Moon data in the following way.

We use a telescopic reflectance spectrum (McCord and Adams, 1973) of the Apollo 16 landing site, which is a bright area in the highlands of the Moon's surface where the albedo is particularly high.

At this point on the Moon the signal is given by:

$$F_{\text{Moon}}(x^*, \lambda) = R_{\text{Moon}}(x^*, \lambda) \times S_{\text{Moon}}(\lambda) \cdot \text{UR}(x^*, \lambda), \tag{1}$$

where R_{Moon} is the lunar spectral reflectance computed at a point x^* in the lunar highlands (see Figure 9), S_{Moon} is the solar radiance at the mean Moon–Sun distance (1 A.U.) and UR is the unknown transfer function at the point x^*. Accordingly, the Unit Response transfer function is:

$$\text{UR}(x^*, \lambda) = \frac{F_{\text{Moon}}(x^*, \lambda)}{R_{\text{Moon}}(\lambda) \times S_{\text{Moon}}(\lambda)} \tag{2}$$

This is the transfer function for the point on the Moon x^* located in the slit center.

In order to obtain a target-independent UR function we have to consider a flat field. Assuming the uniformity of Venus' dayside atmosphere we define a flat field using the ratio between the signal $F_{\text{Venus}}(x, \lambda)$ at some point x in the frame and $F_{\text{Venus}}(x^* = 32, \lambda)$ in the center of the slit.

$$[F_{\text{Venus}}(x, \lambda)]_{\text{Norm}} = \frac{F_{\text{Venus}}(x, \lambda)}{F_{\text{Venus}}(x^*, \lambda)} \tag{3}$$

The signal on Venus is given by an expression analogous to (1) for the Moon:

$$F_{\text{Venus}}(x, \lambda) = \text{UR}(x, \lambda) \times R_{\text{Venus}}(\lambda) \times S_{\text{Venus}}(\lambda) \tag{4}$$

$$F_{\text{Venus}}(x^*, \lambda) = \text{UR}(x^*, \lambda) \times R_{\text{Venus}}(\lambda) \times S_{\text{Venus}}(\lambda) \tag{5}$$

where S_{Venus} is the solar radiance at the mean Venus-Sun distance (0.73 A.U.). Putting (4) and (5) into Equation (3) we obtain the normalized signal on Venus:

$$[F_{\text{Venus}}(x, \lambda)]_{\text{Norm}} = \left[\frac{\text{UR}(x, \lambda)}{\text{UR}(x^*, \lambda)}\right] \tag{6}$$

Using this result it is possible to define the UR as the product of the transfer function computed for the Moon at point x^* (45, 33) and the transfer function normalized to the center x^* of the VIMS-VIS slit on Venus:

$$\text{UR}(x, \lambda) = \text{UR}(x^*, \lambda)_{\text{Moon}} \times [F_{\text{Venus}}(x, \lambda)]_{\text{Norm}} \tag{7}$$

Finally, we obtain the general UR:

$$\text{UR}(x, \lambda) = \text{UR}(x^*, \lambda)_{\text{Moon}} \times \left[\frac{\text{UR}(x, \lambda)}{\text{UR}(x^*, \lambda)}\right]_{\text{Venus}} \tag{8}$$

Figure 10 shows the final UR transfer function for all the wavelengths: note that the UR is a function of the pixel position. The UR function permits conversion of DN to physical units.

6.2.3. *Conclusions*

Additional radiometric calibration improvements are expected as the Jupiter encounter data are analyzed and compared with the ground calibration results (see McCord *et al*., 2004). During Cassini's Saturn tour, there will be many measurements for a variety of objects that will help identify and allow removal of any remaining artifacts in the spectral radiometric calibration. Users of VIMS data should consult later papers by the investigation team, as well as the VIMS website, for the most current versions of the calibration of the instrument.

6.3. Geometric Calibration

For VIMS, the primary data product is, for each resolved pixel of a given target, the determination of both the pixel position and the full spectrum from 0.35 to 5.1 μm. To build such spectral images, for each picture element of any given 64 $\times$ 64 frame, the viewing direction of each of its 352 contiguous spectral elements (spectels) must be known. Thus, the prime goal of the geometric calibration of VIMS was to determine the relative viewing directions of all 96 VIMS-VIS and 256 VIMS-IR spectels within the full VIMS field of view (FOV), in a frame to be referenced to the Cassini spacecraft.

VIMS-VIS and VIMS-IR form images in two distinct ways. VIMS-VIS operates like a push-broom, acquiring an entire cross-track line simultaneously spread over

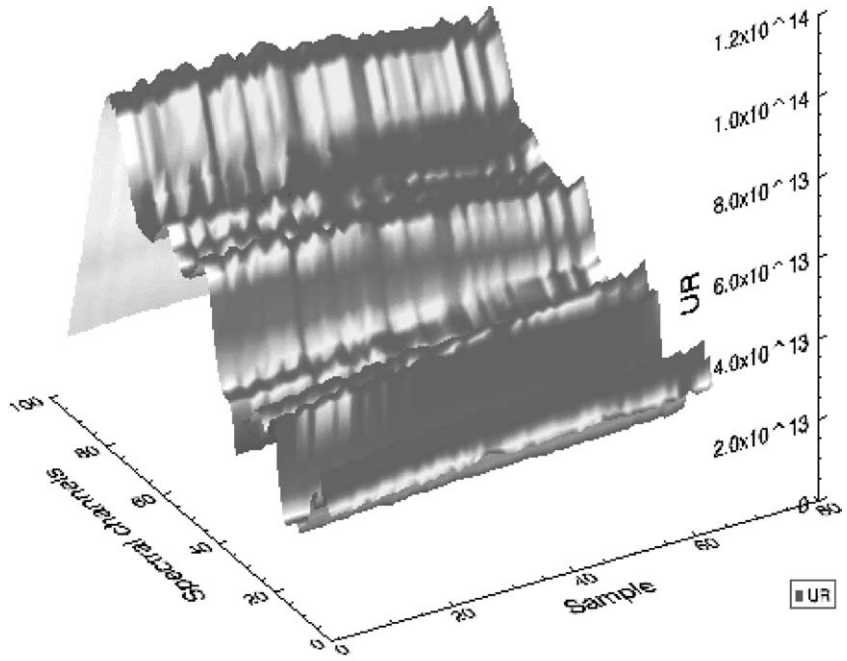

Figure 10. The computed UR transfer function.

its spectral dimension (from 0.35 to 1.0 μm) along the second dimension of its CCD detector. The second spatial dimension is acquired either using the spacecraft drift or the scanning of the VIMS-VIS telescope secondary mirror. VIMS-IR uses only a linear array detector, thus it acquires one pixel only spread over its spectral dimension (from 0.85 to 5.1 μm). The cross-track spatial dimension is acquired by scanning the telescope secondary mirror (whiskbroom mode), while the along track dimension is acquired (as for VIMS-VIS) using either spacecraft drift or scanning the IR telescope's secondary mirror in the second dimension. With two distinct scanning mechanisms, telescopes, and spectrometers, the boresight alignment and the Instantaneous Fields Of View (IFOV) within the full FOV are not identical by design, and, in principle, are wavelength dependent. The geometric calibration is thus intimately coupled to the determination of these spectral registration effects.

Due to the late delivery of VIMS-VIS, the ground geometric calibration was performed in steps: the in-depth geometric calibration of VIMS-IR was performed first, prior to the integration with VIMS-VIS, followed by the geometric calibration of VIMS-VIS after its integration. After integration, a large misalignment was observed, requiring a global mechanical realignment of both the IR and V channels (out of the calibration chamber), followed by a few final control measurements (back to the calibration chamber) prior to integration with the Cassini spacecraft. Some in-flight calibrations were performed to assess the actual geometrical characteristics of

both channels, when the instrument had reached its proper in-flight thermal regime, late during the cruise towards Jupiter.

During the ground calibration, VIMS was mounted on a fixed platform, thermally controlled and under vacuum. A collimator and optical bench assembly was constructed outside of the thermal-vacuum chamber, and viewed through a large window. For the geometric calibration, we chose to image with VIMS, two types of targets, both mounted on an X–Y stage to allow coverage of the entire VIMS FOV. In the target projector plane, one VIMS pixel (0.5 mrad) corresponded to $\sim$1 mm. To cover the entire VIMS FOV, the target was 64 mm in size, and the stage was moved by steps of 0.1 mm (1/10 VIMS pixel). The first type of target consisted of linear blades to measure potential spectral registration effects by analyzing for each spectel the pixel response while the blade was moved across the pixel. The other target placed in the projector focal plane consisted of an opaque metal plate with a grid of sub-pixel sized pinholes (0.1 mm in diameter) evenly spaced, and back-illuminated by a tungsten lamp. The complete calibration data products are in the form of tables, one for each spectral channel, giving the viewing direction of each VIMS pixel. Below we summarize some of the main results.

The IFOVs of both channels were accurately measured. Averaged over all wavelengths within a given channel, $\mathrm{IFOV_{IR}} = 0.495 \pm 0.003$ mrad, and $\mathrm{IFOV}_{VIS} = 0.506 \pm 0.003$ mrad. Although the differences appear small ($\sim$2%), they result in a misalignment of VIMS-VIS relative to VIMS-IR of more than one pixel over the 64-pixel FOV. This imposes the need for a thorough geometric re-sampling of all image cubes larger than 32 pixels. Prior to launch, the last geometric measurement showed a boresight alignment between VIMS-VIS and VIMS-IR of better than 0.3 pixels at all wavelengths. Images coincide independent of wavelength to within $<$0.5 pixel in frames up to 12 $\times$ 12 pixels.

The first measurements in flight were performed using both channels to observe the Moon during the Cassini Earth-Moon fly-by (August 18, 1999). Those showed a boresight misalignment of VIMS-IR with respect to VIMS-VIS $\Delta(X, \Delta Y) = (-1$ pixels, $(+2$ pixels). Because the VIMS-IR was warmer than its proper operating temperature at the time of the Earth–Moon flyby, it was concluded that at least part of misalignment resulted from thermal gradients in the IR channel that would lessen as the Cassini spacecraft moved farther from the Sun and the IR channel cooled. A more recent calibration using the Pleiades cluster and the star Fomalhaut (late March, 2001) showed boresight offsets of $(\Delta X,\Delta Y) = (-1,0)$ pixels. The Pleiades observation (Figure 11) demonstrates the misalignment variation within the FOV, showing the various stars in the visual (blue pixels, averaged over the first 30 VIS spectels) and the near IR (red pixels, averaged over the first 40 spectels).

The ground calibration yielded the VIMS-IR FOV for most IR spectels, leading to spectral geometric registration maps. For images up to 32 $\times$ 32 pixels, all spectral images coincide to better than 1/3 pixel. Larger discrepancies appear in the bottom right and top left corners of the frame, where spectral misalignments up to half a pixel are present. This is illustrated in Figure 12, scaled in mrad, for

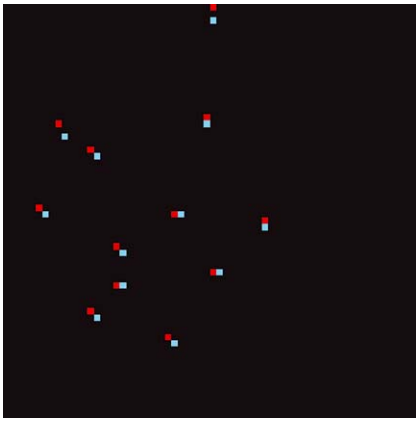

Figure 11. VIMS image of the Pleiades, showing the stars in the VIMS-VIS (blue pixels) and the VIMS-IR (red).

three IR wavelengths (spectels 103, 150 and 206, at 0.98 μm, 1.75 μm and 2.68 μm, in red, blue and green respectively), enlarging the four corners and the center of the FOV geometric spectral responses. Finally, the spectral registration effects measured for the IR spectels were demonstrated to be very low, as illustrated in the figure: the very high sensitivity of the measurements allows detection of effects at a scale smaller than 1/10 pixel. With this resolution, the larger effects we see between contiguous spectels actually amount to 1/10 pixel, and in fact result from atmospheric contributions during the calibration (variation of H_2O and CO_2 features). The only large-scale effect present (black curve) has a very low frequency (at the scale of the entire spectral range), and likely results optical aberrations within the IR spectrometer. It is both smooth and small enough to minimize the risk of misinterpreting potential large optical contrasts in the observed scene in terms of false spectral signatures.

6.4. Spectral Calibration

6.4.1. *Summary of Tests*

The goals of the spectral calibration of VIMS were to measure the spectral response of each VIMS spectral channel to determine the central wavelength and spectral profile of each detector, and its spectral stability as a function of temperature and spatial position within the field of view of the instrument. To achieve this, the tests included: (1) scanning a nearly monochromatic line (using a calibrated grating monochrometer) over the VIMS wavelength range to map the spectral profile of each VIMS detector, (2) transmission spectra of materials with sharp absorption bands, and (3) measuring reflectance spectra of minerals and other targets with VIMS.

The monochrometer scans were useful for a single position in the full VIMS field of view because the relatively large field of view of the VIMS could not be covered

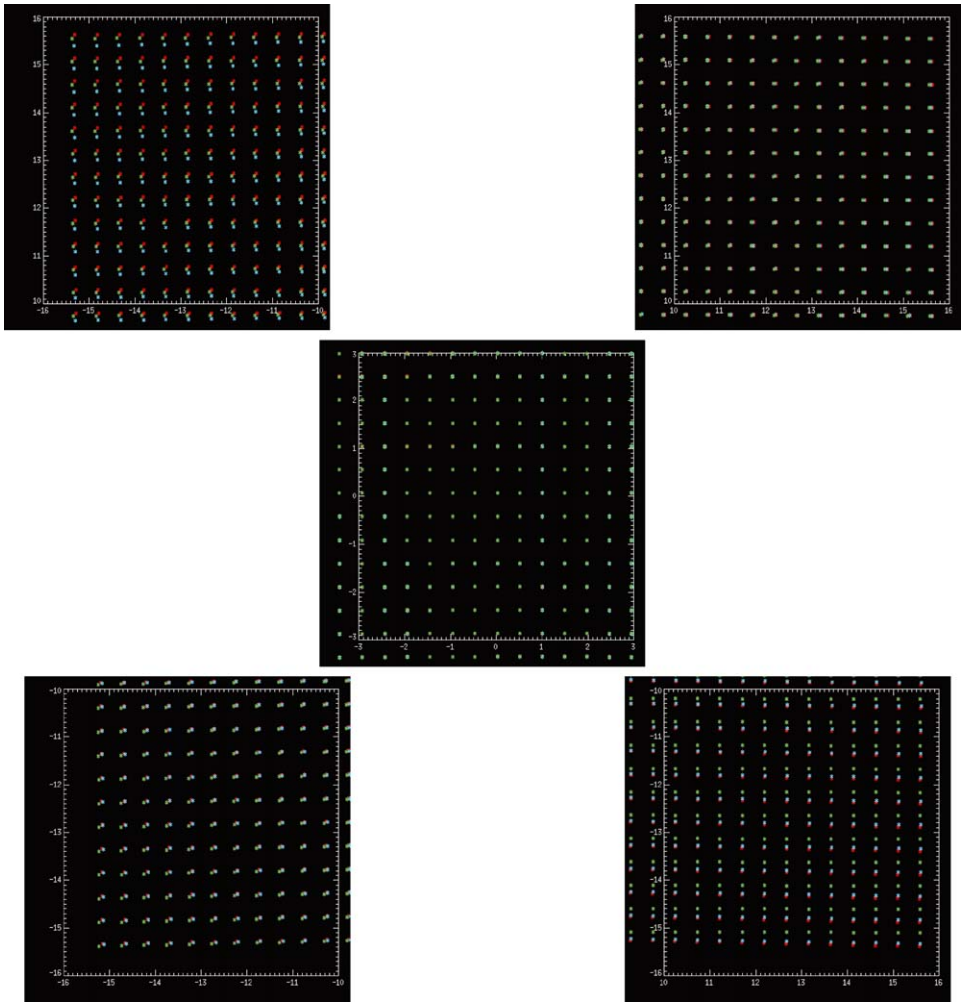

Figure 12. Spectral registration maps for five positions in the VIMS field of view. The position of each panel in the instrument focal plane can be seen from the coordinates in each square frame. The vertical and horizontal directions (relative to the upper left) correspond to the +Z and +X axes of the spacecraft coordinate system.

with the narrow exit slit of the monochrometer, and small shifts in wavelength were observed in the monochrometer as a function of position along the slit. This results because a change in direction along the slit results in a slight change in the field position in VIMS that corresponds to an angular movement. Such changes require a change in the light path through the monochrometer with a corresponding change in the effective output wavelength of the monochrometer. Thus the monochrometer tests were done on-axis only. The monochrometer was typically scanned at 1 nm increments to map out the profile of each VIMS spectral bandpass.

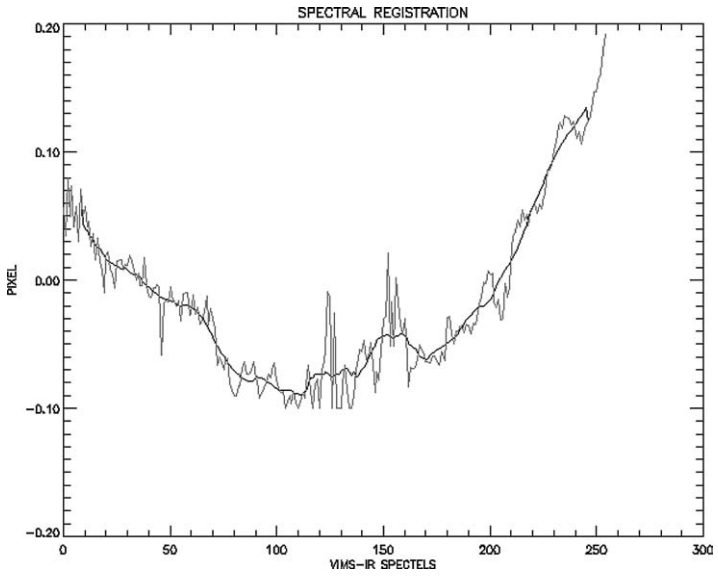

Figure 13. Plot of the deviation (calculated versus actual) for the pointing direction (in the direction of the boresight) as a function of wavelength (shown as spectel, or channel number). As examples, in the direction of the boresight, the IFOV of spectel number 1 deviates by +0.006 pixel, while spectel number 115 deviates by −0.08 pixel.

Calibrated transmission filters consisting of a mylar sheet displaying sharp absorption bands in the 1–3.5 μm region, with broader features at longer wavelengths, and Corning glass filters containing rare-earth elements which give sharp absorption features in the visual and near-infrared wavelength regions, and broader absorptions at longer wavelengths were used to cover the full VIMS field of view. Because of their uniformity and stability, the filters were used to determine the stability of the VIMS wavelength response as a function of spatial position, temperature, and time (because two tests were done over a period of about six months).

To measure the response of VIMS to real targets with spectral features, a set of minerals and other materials were assembled into a spectral target and measured in reflectance. Because the calibration geometry was optimized for other tests, the setup for reflectance measurements was not ideal, so these tests were qualitative. The light source used to illuminate the samples was set up at relatively large angles to the normal to the surface of the highly scattering surface of the spectral target, but the exact viewing geometry was difficult to control. Furthermore, only samples mounted vertically could be measured, so it was not possible to measure the reflectance of unconstrained, loose particulate samples. Measurements were made of rocks and solid samples that typically had large grains, thus the absorption bands were deep and saturated, but the spectra of these rocks are quite identifiable with VIMS.

The spectral calibration tests showed that VIMS is a remarkable instrument, producing spectra comparable in quality to specialized laboratory spectrometers.

The large spectral range of the VIMS includes the region of increasing thermal emission at room temperature $\lambda \geq 3\mu$m) making the light reflected from the sample difficult to separate from the background thermal emission. The spectral range of VIMS is greater than the spectral output any single convenient laboratory light source, so tests were often done multiple times with different light sources.

6.4.2. *Spectral Profiles*

The VIMS-IR spectral profiles are very close to Gaussian in shape, with small, Gaussian shaped side lobes (Figures 14a and 14b). The small side lobes are possibly caused by reflections in the order sorting filters. The side lobes are stronger on the short wavelength side at the short-wavelength end of the IR array, and are stronger on the long wavelength side on the long-wavelength end of the array. The side lobes are typically 2% or less of the strength of the central profile and can probably be ignored except for the most rigorous work. A set of spectral profiles for each spectral channel will be maintained on the Cassini VIMS team home page. Spectral profiles are somewhat distorted near the VIMS order-sorting filter gaps. These gaps occur at VIMS-IR channels 45–46, 128–129, and 183–183 (1.59, 2.96, and 3.86 μm). At or near the filter gaps, the central portion of the spectral profile can be absorbed, leaving the main signal coming from the side lobes (Figure 15). Except for the side lobes, no out-of band signals were detected in the monochrometer scans.

6.4.3. *Cruise Spectral Calibration*

During cruise, high signal-to-noise spectra were obtained on the Moon, stars, Jupiter, and the Galilean satellites. Immediately apparent in these cruise data is that the wavelengths of VIMS-IR shifted after launch. A best fit that shows overlap consistency between VIMS-VIS and VIMS-IR using deep absorption bands in the spectra of Jupiter shows a 1.3 channel ($\sim$21 nm) shift in the IR wavelengths (Figure 16). The positions of absorption features in sub-pixel images of stars and the Galilean Satellites showed variability by up to 1/3 channel depending upon where the object was located in the slit. This adds difficulty in determining the wavelength calibration post launch to better than about 5 nm. Despite this difficulty, comparison with the Galileo NIMS data on the Galilean satellites confirms the 1.3 channel shift at the positions of the 4.25-μm CO_2 feature and water–ice absorptions seen in spectra of Ganymede and Callisto. Analysis of absorption features throughout the VIMS-IR spectral range shows that the shift is consistent across the entire wavelength range of VIMS-IR. Calibrations using stars and other objects will be performed frequently throughout cruise and the orbital tour.

6.5. Polarimetric Calibration

The VIMS instrument contains no specific polarimetric capability, such as filters or grids, but the design of the grating spectrometer makes it inevitable that the instrument's response will be linearly polarized to some extent. The purpose of the

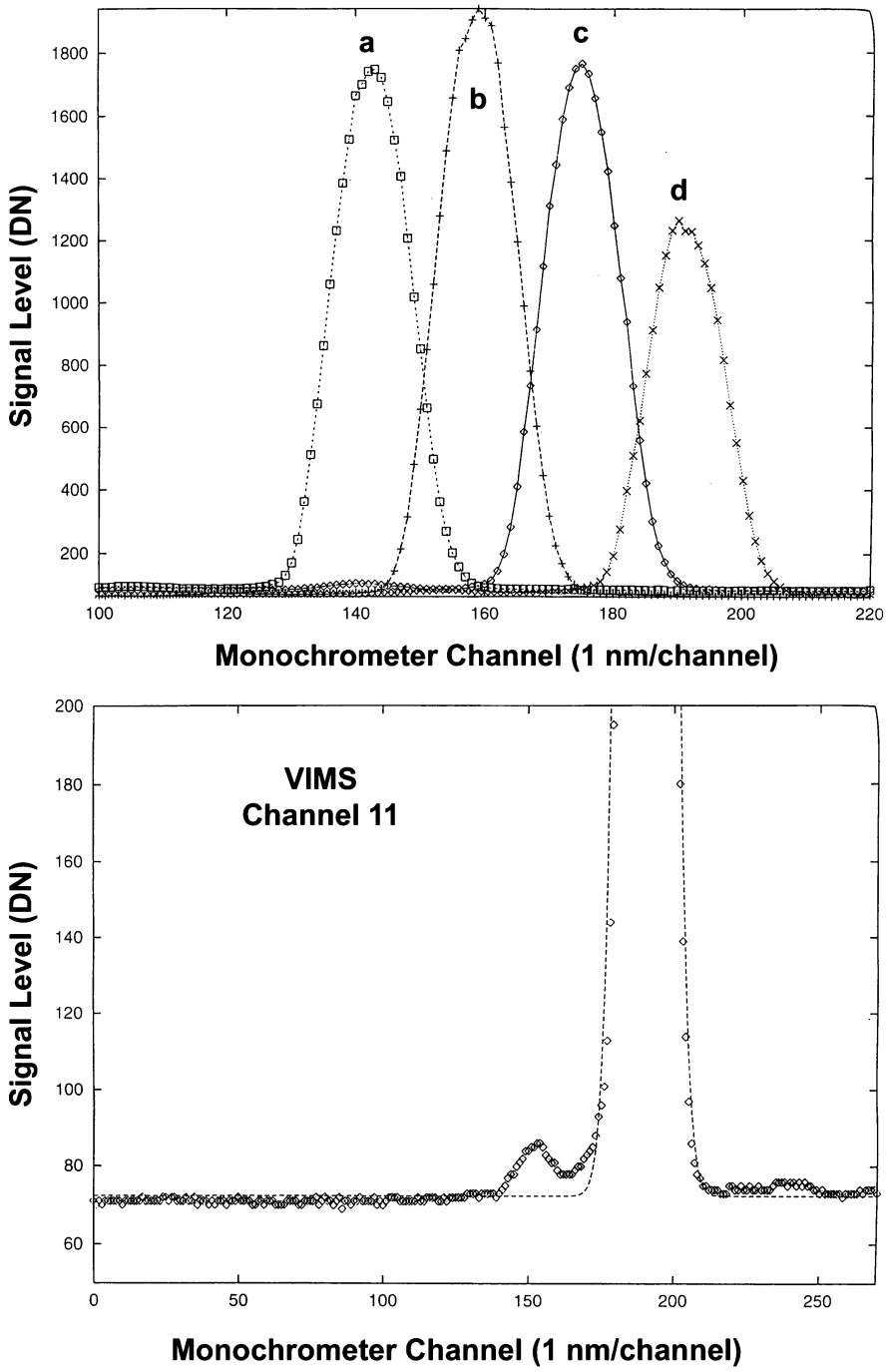

Figure 14. (a) VIMS-IR spectral profile at several wavelengths. (b) Enlargement of one profile to show the small side lobes.

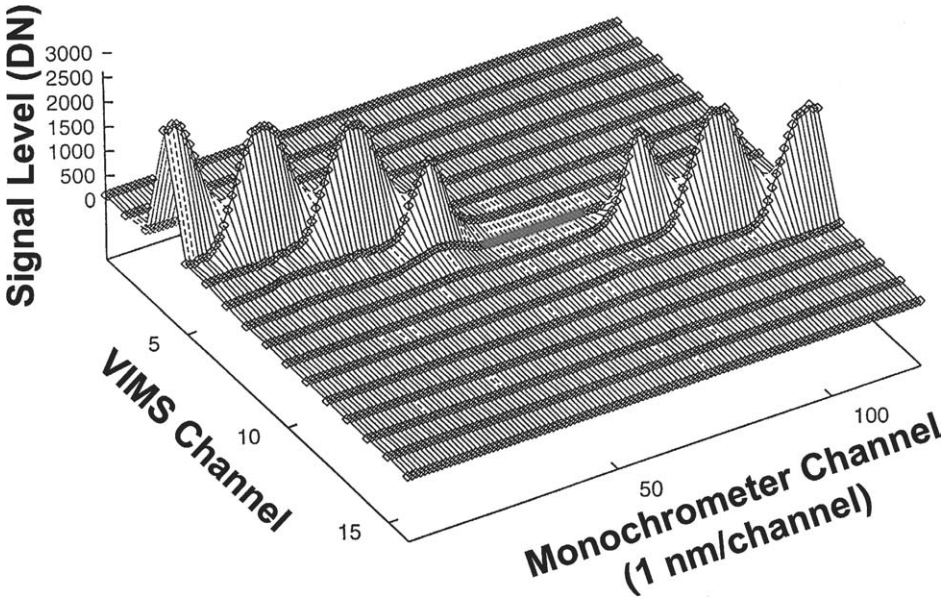

Figure 15. Monochromatic spectral image profiles for VIMS-IR near the filter gaps, as noted in the text.

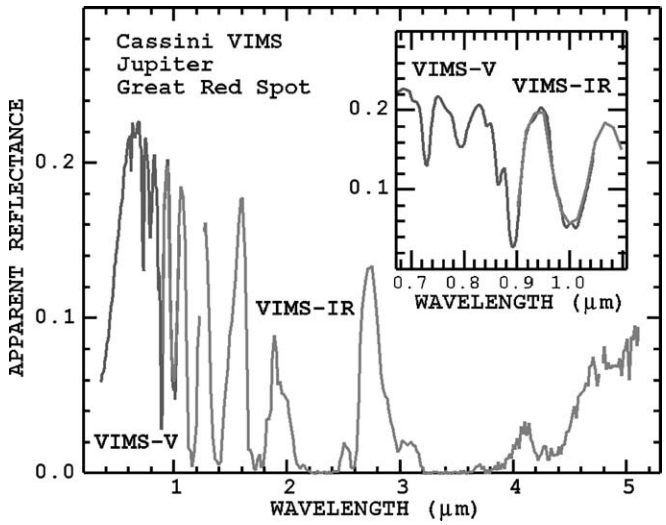

Figure 16. Spectra of Jupiter with VIMS-VIS and VIMS-IR. The inset shows an enlargement of the region of spectral overlap.

polarimetric calibrations was to characterize this sensitivity, so that its effect on the accuracy of spectra obtained for both polarized and non-polarized targets in the Saturnian system can be assessed. In general, spacecraft pointing constraints will determine the roll attitude of the optical remote sensing instruments during

targeted observations, leaving little opportunity for observations at multiple roll orientations.

Measurements for the polarization characterization of VIMS-IR were carried out in the 10-feet thermal-vacuum tank in Building 144 at JPL, during January 17–20, 1996. A target projector was set up with a 26-mm diameter IR linear polarizing filter at the focal plane of a collimator. The target was illuminated by the 1-inch output aperture of an integrating sphere, producing a polarized image of the exit aperture of the sphere at the VIMS focal plane. The polarizer consisted of a ZnSe substrate with a deposited aluminum pattern of parallel stripes, and its polarization efficiency is documented from 2.5 μm to beyond 10 μm. The average single-polarizer throughput is 38%, while the maximum cross-polarized throughput over the 2.5- to 5.0-μm range is 1.5%. No data on the filter transmission were available below 2.5 μm. A calibrated tungsten source with a Teflon-coated sphere provided adequate SNR out to about 2.5 μm, while a glowbar source with a gold integrating sphere provided adequate SNR at all wavelengths beyond 1.5 μm.

Measurements were made at five spatial positions of the source in the target plane, on boresight, and near the four corners of the VIMS field. For each source position, measurements were made at seven settings of the polarizer, at 30 $^\circ$ intervals between ($+90^\circ$ and -90°, followed by a sequence of background measurements with the shutter on the light source closed. Only VIMS-IR was available for these measurements.

Three cubes per measurement were co-added and background-subtraction spectra were extracted both for a central spot in the image of the source and for a larger region which included the full output aperture of the sphere. This was accomplished at each orientation of the polarizer and for each source position.

Figure 17 shows 3-D surface plots of the normalized spectra for both light sources, measured on the boresight. At each wavelength, the measured intensity at a particular polarizer angle was divided by the average over all seven positions. From this figure, and similar ones constructed for other source positions, it is apparent that the maximum signal invariably occurs at an orientation of either 0 $^\circ$ (polarizer parallel to the rulings on the grating) or 90 $^\circ$, but that the sense and magnitude of the polarized response vary smoothly with wavelength. We thus calculated the fractional polarization of VIMS-IR from the expression:

$$P(\lambda, \%) = \frac{2I(\lambda, 0^\circ) - I(\lambda, -90^\circ) - I(\lambda, +90^\circ)}{2I(\lambda, 0^\circ) + I(\lambda, -90^\circ) + I(\lambda, +90^\circ)} \times 100$$

Figure 18 shows the polarization determined from central-spot and full-aperture data from both sources, at two locations in the VIMS FOV. The results were found to be the same to within 1% or better for all source positions and aperture sizes, and essentially identical for both tungsten and glowbar sources in their region of overlap (1.2–2.5 μm).

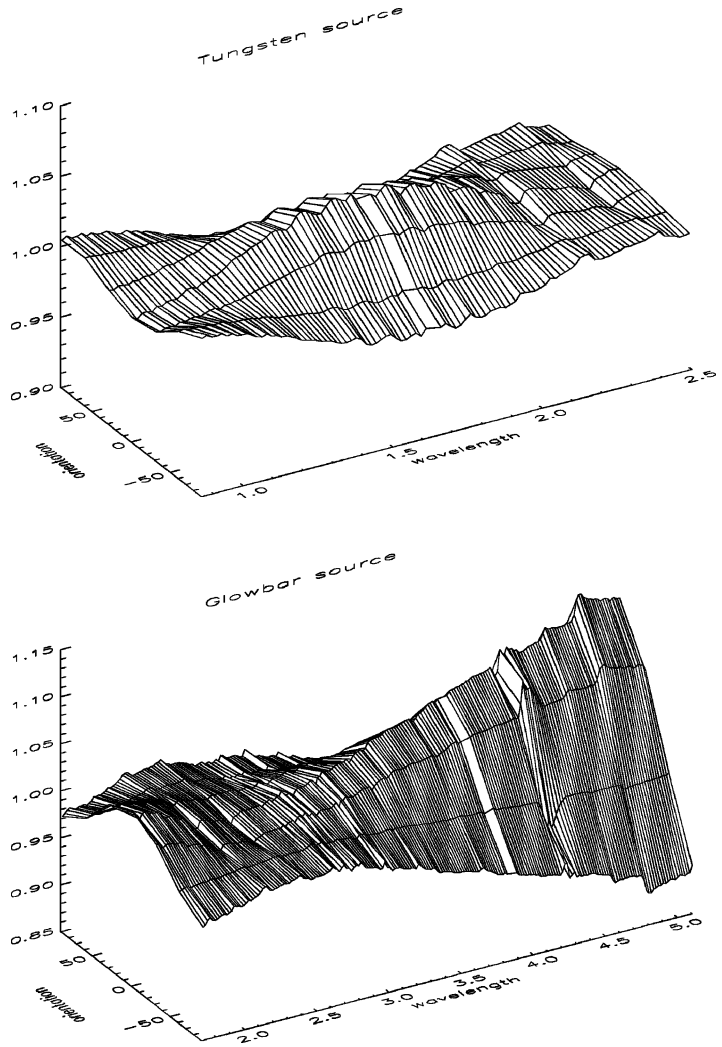

Figure 17. 3D surface plots of VIMS polarization measurements.

In summary, the calibration data showed the following:

1. The maximum polarization sensitivity is either parallel to (positive) or perpendicular to (negative) the rulings on the diffraction grating.
2. The polarization is positive for wavelengths of 1.1–2.1 μm, and beyond 2.4 μm, but negative below 1.1 μm. Between 2.1 and 2.4 μm the polarization is negligible (less than 1%). A peak in polarization occurs at 1.6 μm (+3%). Beyond 2.5 μm, the polarization increases linearly with wavelength, reaching a maximum of about 11% at 5.0 μm.

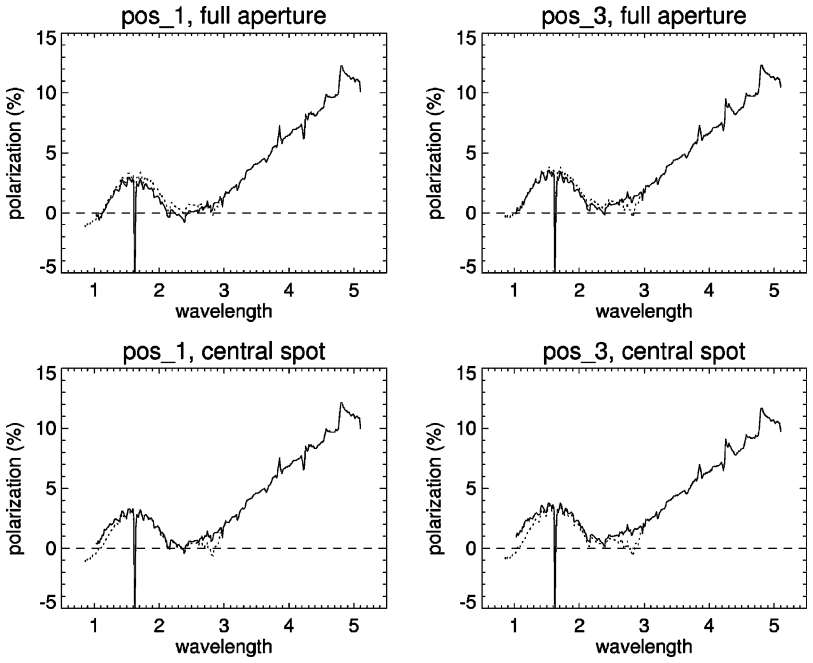

Figure 18. Results of polarization measurements.

3. Except for some artifacts at the segment boundaries of the blocking filter at 1.6 and 3.9 μm, the level of polarization is continuous, suggesting that the polarization is not related to the filter.
4. The lack of a significant dependence of polarization on the particular light source used indicates that the origin of the polarization is not in the sources, although it could conceivably be in the window of the thermal-vacuum chamber.
5. The lack of variation of polarization with target position suggests that the polarization does not arise from the VIMS scan mirror.

These results suggest that the origin of the measured polarization is within the spectrometer, and most likely resides in the diffraction grating. Measurements of the ZnSe chamber window indicate no significant polarization, at least at wavelengths below 1.7 μm.

To assess the implications for spectral observations, consider a source with a fractional linear polarization f in a direction è with respect to the VIMS "zero angle", as defined above. The parallel and perpendicular components of the incident intensity are then:

$$I_{\text{par}} = [0.5 + f\cos^2\theta]I_0 \text{ and } I_{\text{perp}} = [0.5 + f\sin^2\theta]I_0$$

The measured intensity of the source by VIMS is:

$$I(\theta) = (1 + P)I_{\text{par}} + (1 - P)I_{\text{perp}} = [1.0 + f + Pf\cos(2\theta)]I_0$$

The RMS fractional error in a single measurement of the intensity at an arbitrary orientation is:

$$\frac{\sigma(I)}{< I >} = \frac{Pf}{\sqrt{2(1+f)}}$$

For the most severe case of P = 11% (Figure 18), the RMS error is <1% for $f < 0.15$, which probably includes any natural source polarization likely to be encountered. At wavelengths below 3.3 μm, the error will reach 1% only for $f = 0.9$, and is thus almost certainly negligible.

6.6. Solar Port Calibration

6.6.1. *Ground Calibration*

The solar calibration port (henceforth "cal port") was installed within the VIMS-IR telescope to provide a strongly attenuated spectrum of the Sun during the Cassini mission, which facilitates reduction of VIMS spectra to an accurate scale of absolute reflectance. The cal port axis is offset by 20 ° from the telescope boresight in the $-Z$ direction, aligned with the UVIS solar occultation port. Attenuation of the incident solar beam by a factor of $\sim 2.5 - 10^7$ is achieved by (i) the small aperture of the cal port, compared to the main beam and (ii) a series of one 70 ° and five 90 ° reflections from right-angle prisms made of ZnSe. Most of the incident flux is directed back through the entrance aperture by internal reflection in the prisms. The beam exiting the cal port is focused by the telescope optics onto the VIMS-IR entrance slit, and then enters the spectrometer in the same way. But because the cal port aperture samples only a portion (~0.3%) of the full instrument aperture, the collimated beam illuminates only a small part of the diffraction grating. The optical design ensures that this region overlaps the short- and medium-wavelength blaze regions on the grating, in the ratio 1:3. The cal port does not illuminate the long-wavelength blaze.

The predicted throughput of the stack of prisms varies smoothly from 1.35×10^{-4} at 0.85 μm to 1.09×10^{-4} at 3.0 μm and 1.04×10^{-4} at 5.0 μm, for radiation linearly polarized in a plane perpendicular to the plane containing the incident and exit beams and to the rulings on the VIMS diffraction grating. The transmission of the orthogonal polarization is less than 1.0×10^{-7}. The output spectrum of a target seen through the cal port differs from that produced by the same source seen on the instrument boresight. This arises through a combination of polarization and partial illumination of the grating. Partial illumination of the grating results in a different set of contributions from the different blazes than occurs when the grating is fully illuminated. The purpose of the cal port calibrations is to establish the ratio of the spectrum of an unpolarized broadband source as seen through the cal port to that of the same source on the instrument boresight.

The simulated solar source used for the calibration runs was a high-power xenon lamp, illuminating a large, white, teflon-coated integrating sphere. The output of the sphere illuminated a 1-mrad diameter circular aperture in the focal plane of

the calibration projector (equal to the angular size of the sun at 9 AU), after a 90° reflection from an aluminum plate. One side of this plate was polished and oriented for specular reflection of the high-intensity beam onto the target for the cal port runs, while the other was sand-blasted to provide diffuse reflected illumination of the target for the boresight runs.

All measurements were made on July 12, 1996, in the 10-feet thermal-vacuum chamber at JPL. Inside the tank, a deployable periscope-like arrangement with two aluminum mirrors was used to redirect the input beam into the cal port's entrance aperture. The input signal to VIMS thus experienced identical atmospheric paths, with the same number of reflections, for both cal port and boresight runs. For each observation multiple 8×8 image cubes were taken, centered manually on the image of the target. Only VIMS-IR was available for these runs; VIS-VIS was calibrated separately at Officine Galileo.

A total of 100 separate cal port image cubes were background subtracted and averaged in sets of ten, and all pixels co-added to produce spectra. Twenty boresight cubes were processed in identical fashion. Figure 19 shows the average boresight and solar port spectra, at the DN levels originally recorded. The resulting ratio spectrum is displayed in Figure 20, normalized to an average value of unity. Data for nine channels at the three filter segment boundaries have been interpolated in both plots.

The ratio spectrum shows that the cal port sensitivity is relatively low shortward of VIMS-IR channel 50 (1.7 μm), increases rapidly between channels 50 and 70 to a peak at channel 80 (2.2 μm), and then declines smoothly at longer wavelengths. Oscillations near 2.7 and 4.3 μm are due to imperfect cancellation of CO_2 absorption features in the raw spectra. The high-frequency structure beyond of 4.0 μm is an artifact of the array readout.

The decline in sensitivity of the cal port relative to the main aperture at longer wavelengths is attributable to the lack of illumination of the long-wavelength grating blaze, and to the increasing polarization sensitivity of the VIMS-IR beyond 3 μm. The steep drop shortward of 2 μm is, on the other hand, unexplained. Neither the ZnSe prisms nor the several aluminum reflections seem to be capable of causing this effect. Additional experiments showed no indication of a misalignment in the projector illumination pattern. Previous calibration runs on June 26, 1996, which did not use the external Al plate, did not achieve sufficient SNR at the longer wavelengths. Nevertheless, these earlier results are not consistent with the final runs at short wavelengths, for reasons that are presently unknown. Thus, the cal port ratio spectrum in Figure 20 must be considered provisional, until in-flight experience is available.

Viewed through the VIMS-IR cal port, images of a circular target are noticeably elongated. FWHM dimensions are $\sim$2.0 pixels in X, but increase steadily from 2.8 pixels in the Z direction at 1 μm to 4.1 pixels at 5 μm. This may be compared with FWHM sizes for the boresight images of 1.5×2.2 pixels for the same target. The elongation of the solar port images is due to diffraction at the elongated rectangular

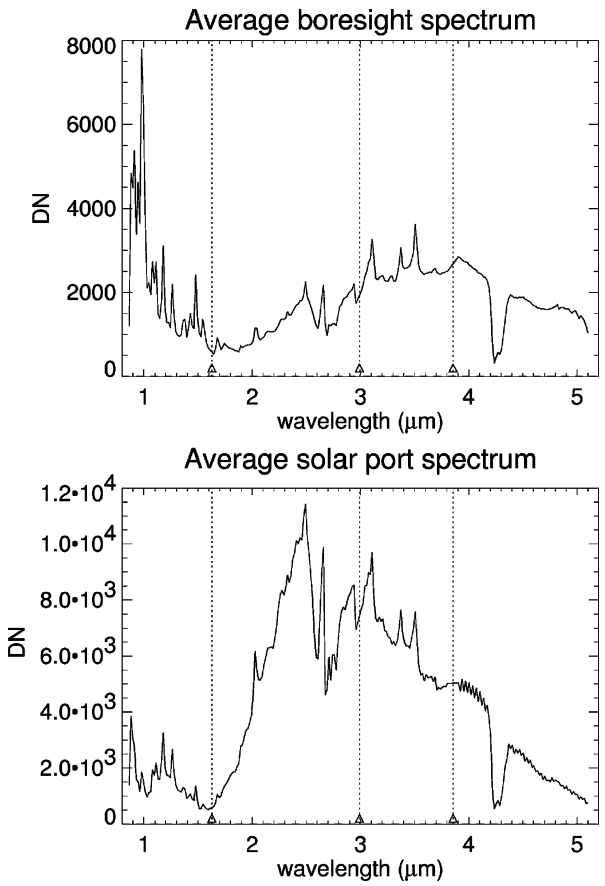

Figure 19. Average instrumental response through the boresight and solar port.

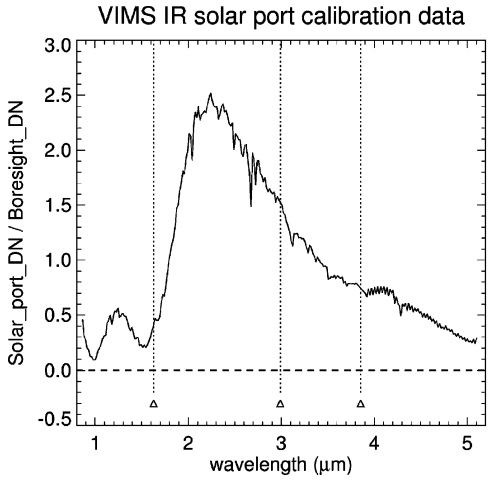

Figure 20. Ratio of response, solar calibration port (cal port) to boresight.

aperture of the cal port (30 mm × 5 mm). Image centroids are fairly stable, varying in X by at most 0.3 pixels and in Z by at most 0.2 pixels. Because of the variable size and slightly wavelength-dependent position of the solar image, it is recommended that solar cal port images be co-added over at least an 8 × 8 pixel region in order to obtain a stable, well-defined spectrum. In-flight observations show that the solar calibration ports in VIMS-VIS and VIMS-IR are co-aligned to within 1 pixel, but offset by 10 mrad from the nominal pointing. This is well within the capability of the VIMS scan mirrors to correct, and will thus permit simultaneous solar occultation measurements with the UVIS instrument.

6.6.2. *Results from Earth–Moon Flyby*

Due to the large attenuation factors incorporated in the design of the VIMS-VIS and VIMS-IR solar calibration ports, the only targets suitable for calibration observations after launch were Venus and the Moon. Prior to the Earth–Moon flyby and the deployment of the VIMS-IR covers, only the VIMS-VIS was operational. Although a short series of observations of Venus through the VIMS-VIS solar port was attempted during the V2 flyby on 24 June 1999, a software error prevented their successful execution. It appears, however, that light from Venus inadvertently entered the solar port during pre-encounter background calibration frames.

Approximately 95 min after Earth's close approach on 18 August 1999, the crescent Moon passed through the field of view of the VIMS solar port. Because full pointing control of the spacecraft was not possible at this time, actual data collection was limited to the period of ∼5 min. during which the Moon crossed the VIMS look direction. The observations were made in image mode, with the slits oriented perpendicular to the direction of the Moon's apparent motion across the focal plane (at 1.32 mrad/min), and with a VIS integration time of 20/sline and an IR integration time of 320 ms/pixel. A total of four full 64 × 64 pixel image cubes were obtained over a period of 91 min, centered on the predicted observation time. Because the VIMS slow-scan direction is towards Z, and the Moon was drifting towards $-Z$, the Moon was expected to cross the spectrometer entrance slits in 2.8 min., with the lit crescent visible for perhaps one min.

The VIMS-VIS solar calibration port did indeed apparently detect the Moon in two successive 20 s. integrations acquired at approx. 5:13 UT, at an average signal level of 22 ± 4 DN above the local sky background. At a distance of 460,000 km, the lunar diameter subtended 7.6 mrad, or 15 VIMS pixels, and the lit crescent completely filled the width of the 0.5 mrad entrance slit. Nevertheless, the design of the cal port prism diffuses the light uniformly along the slit, so no actual image was obtained. Figure 21 shows the resulting spectrum, averaged over all 64 spatial pixels along the slit and over both integrations. Plotted with the solar port spectrum is a spectrum of the bright lunar limb acquired by VIMS-VIS through its main aperture, suitably scaled. Although the illumination direction is the same for both spectra, it should be noted that the cal port observations were obtained at a phase angle of 110°, whereas the boresight spectrum was obtained at 90°.

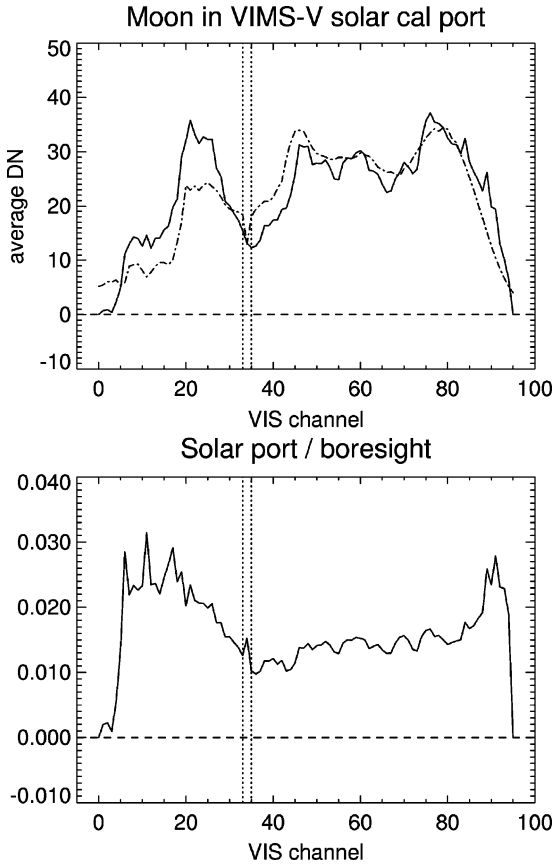

Figure 21. Solar port calibration at the Earth-Moon flyby.

The lower panel of Figure 21 shows that the ratio of lunar spectra obtained through the cal port and on boresight varies relatively smoothly with wavelength (within the SNR limitations of the data), and is highest in the UV. A rough estimate of the overall average attenuation by the VIMS-VIS cal port, taking into account the different integration times and instrument gain states, is,

$$R = \left(\frac{22\text{DN}}{1000\text{DN}}\right)\left(\frac{0.32s}{20s}\right) \times \left(\frac{1}{8}\right) = 4.5 \times 10^{-5}$$

at an effective wavelength of ∼650 nm. Unfortunately, all of the IR data were saturated because both the detector array and the entire spectrometer were too warm.

Although the data obtained at the Moon are of insufficient SNR to use for calibration purposes, they are valuable in (i) demonstrating the functionality of the VIMS-VIS cal port, (ii) confirming the validity of the ground calibration data in, and (iii) providing a basis for estimating solar exposure times at Saturn.

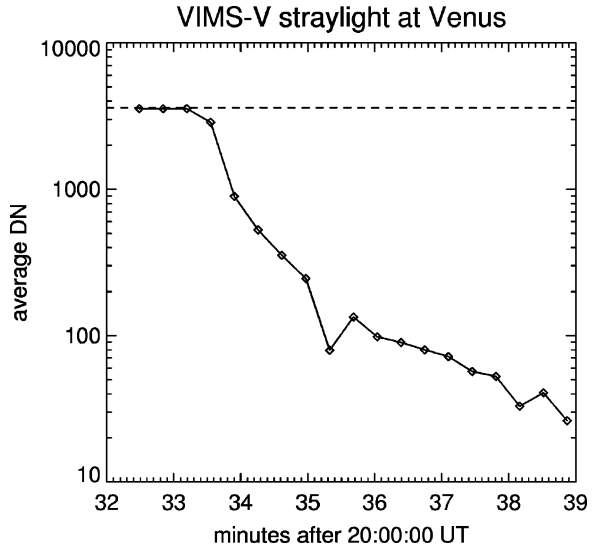

Figure 22. Scattered light measurements at Venus.

6.7. Scattered Light Measurements for the Visual Channel

The Venus 2 flyby on June 24, 1999 provided an excellent opportunity for measurements of scattered light from a very bright off-axis source. Twenty seven integrations were executed by VIMS-VIS shortly after Venus close-approach, and immediately after the VIMS boresight moved off the bright limb of the planet onto dark sky. Operating in line mode with an integration time of 20 s, these observations spanned the period 20:32:29–20:42 UT and commenced with the VIMS boresight pointed 4.9° away from the nearest point on Venus' limb.

Data from the first three integrations, within 10° of the limb, are saturated in all 96 spectral channels and all 64 spatial pixels along the slit. Subsequent integrations show scattered light rapidly declining, as shown in Figure 22, until the sky background level was reached at around 20:39 UT. The signal had fallen by a factor of 10 by 20:35, when the VIMS boresight was pointed 23.2° off the limb.

Throughout the scattered light observations, the recorded spectrum remained essentially unchanged except for the absolute level, as shown in Figure 23. This spectrum, however, is virtually flat and does not show the characteristic spectral response of VIMS-VIS to broadband solar radiation, such as was observed at Venus and the Moon. The feature at channel 34 (∼600 nm) is due to partial obscuration of the focal plane array at the segment boundary between the short- and long-wavelength blocking filters.

Further analysis strongly suggests that the measured signal is due to off-axis light from Venus which entered the entrance slit of the spectrometer enclosure directly (passing just above the fold mirror M2), without reflecting off the scanning

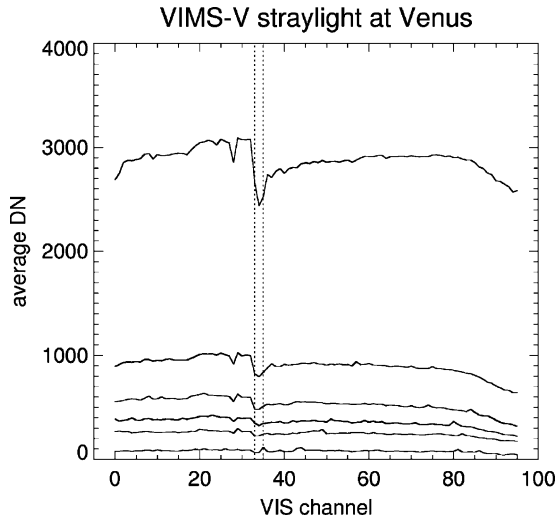

Figure 23. Non dispersed stray light.

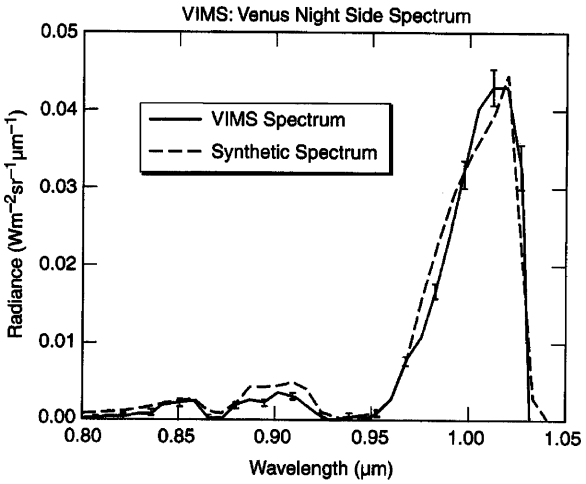

Figure 24. VIMS-VIS spectrum of the night side of Venus, compared to a synthetic spectrum (normalized at 1.01 μm). From Baines *et al.*, 2000.

mirror, and then was reflected by mirror M3 and the collimator directly to the FPA, bypassing the diffraction grating. At the time of the observations, Venus' disk subtended a radius of 55–59 °, and the nearest point on the limb was located within a few degrees of the +Z direction from the VIMS boresight. 3-D ray-tracing indicates that undispersed scattered light may reach the FPA from an off-axis direction of $\sim$17 ° towards $+Z$ and $\pm$10 ° in X, a location which would have fallen on the illuminated disk of Venus over a period which matches that of the observed signal in Figure 22.

A series of similar observations were made just as the VIMS boresight crossed the opposite limb of Venus to probe the planet's night side spectrum. These spectra, obtained when the illuminated disk of Venus was located between −Z and +X, relative to the boresight, and with the terminator 10–15 ° off axis, show no evidence of a significant component of scattered light similar to that in Figure 23.

Although very evident in long integrations, the level of scattered light is in fact fairly modest: at 13 ° from Venus' limb, and accounting for integration time and instrument gain, the measured signal was ∼0.1% of the average flux received directly from Venus. Similar situations are likely to be encountered during some Titan flybys, and perhaps for Saturn observations near periapse, and may warrant corrections for scattered light.

6.8. Venus Surface and Atmosphere

The power of VIMS to make new discoveries was amply demonstrated by the very first planetary spectrum acquired by the instrument (Baines *et al*., 2000). On June 24, 1999, during the Cassini flyby of Venus, the visual channel obtained a single long-duration (10 s) exposure of the planet's night side. This observation was centered near 20 °N. latitude and 60 °E. longitude, and for the first time quantitatively measured Venusian surface emissions at sub-micrometer wavelengths. As shown in Figure 24, the emission profiles of two spectral features predicted by Lecacheux *et al.* (1993) at 0.85 and 0.90 μm were measured. As with other surface emissions previously observed near 1.01, 1.10, and 1.18 μm by ground-based observers and the near-infrared mapping spectrometer (NIMS) onboard the Galileo spacecraft (e.g. Carlson *et al*., 1991, 1993a,b; Crisp *et al*., 1991; Lecacheux *et al*., 1993; Meadows and Crisp, 1996), these features are located in spectral windows devoid of atmospheric absorption through which radiation emitted from the hot (∼740 K) surface passes through the ∼90 bars of CO_2-laden atmosphere into space. This spectrum is the first detection of the 0.90-μm feature. The shorter wavelength feature at 0.85 μm was provisionally detected in a single wavelength channel just above the detection limit by Galileo NIMS (Carlson *et al*., 1991). In contrast, the VIMS spectral profile of this feature spans a wide range of wavelength at high signal-to-noise.

Adding to the previous work of NIMS and groundbased observers, VIMS thus demonstrated that the surface of Venus could be observed in five distinct windows between 0.85 and 1.18 μm. As shown by Baines *et al*. (2000), compositional maps of the surface of Venus may be obtainable from future spacecraft that take advantage of this novel technique to observe the glowing surface of Venus under nighttime conditions. Future observations should take simultaneous measurements of the flux generated at several purely non-gas-absorbing atmospheric wavelengths (e.g. 1.28, 1.74, 2.29 μm) as well as within the five surface-detecting windows, so that the surface spectrum can be corrected for the highly-spatially-variable extinction due to overlying clouds. As previously demonstrated (e.g. Carlson *et al*., 1993a,b), due to the spherical shape and non-absorbing nature of Venus's sulfuric

acid cloud particles, the wavelength-dependent extinction of Venus aerosols can be estimated over a large wavelength range from observations made at relatively long wavelengths (NIMS successfully used 1.73 and 2.4 μm fluxes to determine cloud extinction at 1.18 μm). In the case of VIMS, observations longward of 1.05 μm were unobtainable since the optics cover of VIMS-IR had not been opened as of the Venus encounter, as noted above. Thus, while the relative shape of various surface emission features could be observed by VIMS-VIS, absolute surface fluxes could not be determined. Nevertheless, the distinct advantage VIMS has over previous spectral instruments to the outer planets—in particular, its ability to simultaneously acquire all wavelengths of a spectrum, and its ability to take long exposures (e.g. 10 s here as opposed to enabled VIMS at Venus to make new discoveries with its very first observation, and portends well the making of new discoveries at the mission's major target, the Saturn system.

7. Conclusions

All indications to the writing of this document are that the VIMS instrument in flight has met or exceeded all of its preflight specifications. Measurements have been, and will continue to be, made of the instrument's performance throughout the roughly 6.5 years of Cassini's cruise to Saturn in preparation for the orbital tour. There is every reason to expect VIMS performance will meet or exceed expectations during the Saturn orbital tour, and that the science results produced from VIMS data will be both rich and exciting. It is indeed a privilege for all of the authors of this document to have participated in the VIMS adventure thus far, and we look forward to the exciting discoveries yet to be made at Saturn.

Acknowledgements

The number of people who are responsible for the design, construction, test, launch and operation of the Cassini/Huygens Mission in general, and the VIMS instrument in particular, is truly enormous, and the brilliance of their contributions may sometimes get lost in the glare of the science discoveries that we all hope will result at Saturn. We cannot list them all here, but they know who they are, and the VIMS Science Team especially wants to acknowledge the enabling contributions of all of those bright and dedicated people who created VIMS, and those who are now helping us to operate it. Without them, none of what is possible with VIMS would be possible. Many thanks to all of you and we hope to see you at Saturn.

References

Aptaker, I.: 1982, *SPIE Instrumentation in Astronomy IV Proceedings*, pp. 182–196.

Baines, K. H., Brown, R. H., Matson, D. L., Nelson, R. M., Buratti, B. J., Bibring, J. P., *et al.*: 1992, *Symposium on Titan*, ESA SP-338, pp. 215–219.
Baines, K. H., Bellucci, G., Bibring, J.-P., Brown, R. H., Buratti, B. J., Bussoletti, E., *et al.*: 2000, *Icarus* **148**, 307–311.
Baines, K. H., Carlson, R. W., and Kamp, L. W.: 2002, *Icarus* **159**, 74–94.
Brown, R. H., Baines, K. H., Bellucci, G., Bibring, J.-P., Buratti, B. J., Capaccioni, F., *et al.*: 2003, *Icarus* **164**, 461–470.
Carlson, R. W., Baines, K. H., Kamp, L. W., Weissman, P. R., Smythe, W. D., Ocampo, A. C., *et al.*: 1991, *Science* **253**, 1541–1548.
Carlson, R. W., Baines, K. H., Girard, M., Kamp, L. W., Drossart, P., Encrenaz, T., *et al.*: 1993a, *Proceedings of XXIV Lunar Planetary Science Conference*, 253.
Carlson, R. W., Kamp, L. W., Baines, K. H., Pollack, J. B., Grinspoon, D. H., Encrenaz, T., *et al.*: 1993b, *Planet. Space Sci.* **41**, 477–485.
Crisp, D., Allen, D. A., Grinspoon, D. H., and Pollack, J. B.: 1991, *Science* **253**, 1263–1266.
Green, R. O., Eastwood, M. L., Sarture, C. M., Chrien, T. G., Aronsson, M., Chippendale, B. J., *et al.*: 1998, *Remote Sensing Environ.* **65**, 227–248.
Griffith, C. A. and Owen, T.: 1992, *Symposium on Titan*, ESA SP-338, 199–204.
Lecacheux, J., Drossart, P., Laques, P., Deladerriere, F., and Colas, F.: 1993, *Planet. Space. Sci*. **41**, 543–549.
McCord, T. B. and Adams, J. B.: 1973, *Moon* **7**, 453–474.
McCord, T. B. and the VIMS Team: in press, *Icarus*.
Meadows, V. S. and Crisp, D.: 1996, *J. Geophys. Res.* **101**, 4595–4622.
Miller, E, Klein, G., Juergens, D., Mehaffey, K., Oseas, J., Garcia, R., *et al.*: 1996, *SPIE* **2803**, 206.
Macenka, S.: 1982, *SPIE* **43**, 46.
Meier, R., Smith, B. A., Owen, T. C., and Terrile, R. J.: 2000, *Icarus* **145**, 362–473.
Pollack, J. B., Dalton, J. B., Grinspoon, D., Watson, R. B., Freedman, R., Crisp, D., Allen, D. A., *et al.*: 1993, *Icarus* **103**, 1–42.
Reininger, F., Dami, M., Paolinetti, R., Pieri, S., and Falugiani, S.: 1994, *SPIE* **2198**, 239–250.
Rice, R., Yeh, P., and Miller, W.: 1991, *Algorithms for a Very-High-Speed, Noiseless Encoding Module*. JPL Publication 91-1.
Roos-Serote, M., Drossart, P., Encrenaz, T., Lellouch, E., Carlson, R. W., Baines, K. H., *et al.*: 1999, *J. Geophys. Res. Planets* **103**, 23023–23042.
Roos-Serote, M., Vasavada, A. R., Kamp, L., Drossart, P., Irwin, P., Nixon, C., *et al.*: 2000, *Nature* **405**, 158–160.
Simon-Miller, A. A., Conrath, B., Gierasch, P., and Beebe, R.: 2000, *Icarus* **45**, 454–461.
Stammes, P.: 1992, *Symposium on Titan*, ESA SP-338, pp. 205–210.
Tomasko, M., Pope, S., Kerola, D., Smith, P., and Giver, L.: 1989, *Bull. Amer. Astron. Soc*. **21**, 961–962.